Outlier Detection using Generative Models with Theoretical Performance Guarantees[*]

Jirong Yi[†]   Anh Duc Le[‡]   Tianming Wang[§]   Xiaodong Wu[¶]

Weiyu Xu[‖]

October 29, 2018

Abstract

This paper considers the problem of recovering signals from compressed measurements contaminated with sparse outliers, which has arisen in many applications. In this paper, we propose a generative model neural network approach for reconstructing the ground truth signals under sparse outliers. We propose an iterative alternating direction method of multipliers (ADMM) algorithm for solving the outlier detection problem via ℓ_1 norm minimization, and a gradient descent algorithm for solving the outlier detection problem via squared ℓ_1 norm minimization. We establish the recovery guarantees for reconstruction of signals using generative models in the presence of outliers, and give an upper bound on the number of outliers allowed for recovery. Our results are applicable to both the linear generator neural network and the nonlinear generator neural network with an arbitrary number of layers. We conduct extensive experiments using variational auto-encoder and deep convolutional generative adversarial networks, and the experimental results show that the signals can be successfully reconstructed under outliers using our approach. Our approach outperforms the traditional Lasso and ℓ_2 minimization approach.

Keywords: generative model, outlier detection, recovery guarantees, neural network, nonlinear activation function.

1   Introduction

Recovering signals from its compressed measurements, also called compressed sensing

---

[*]Jirong Yi and Anh Duc Le contribute equally.

[†]Department of Electrical and Computer Engineering, University of Iowa, Iowa City, USA

[‡]Department of Electrical and Computer Engineering, University of Iowa, Iowa City, USA

[§]Institute of Computational Engineering and Sciences, University of Texas, Austin, USA

[¶]Department of Electrical and Computer Engineering, University of Iowa, Iowa City, USA

[‖]Department of Electrical and Computer Engineering, University of Iowa, Iowa City, USA. Corresponding email: weiyu-xu@uiowa.edu

(CS), has found applications in many fields, such as image processing, matrix completion and astronomy [1–8]. In some applications, faulty sensors and malfunctioning measuring system can give us measurements contaminated with outliers or errors [9–12], leading to the problem of recovering the true signal and detecting the outliers from the mixture of them. Specifically, suppose the true signal is $\mathbf{x} \in \mathbb{R}^n$, and the measurement matrix is $\mathcal{M} \in \mathbb{R}^{m \times n}$, then the measurement will be

$$\mathbf{y} = \mathcal{M}\mathbf{x} + \mathbf{e} + \eta, \tag{1.1}$$

where $\mathbf{e} \in \mathbb{R}^m$ is an l-sparse outlier vector due to sensor failure or system malfunctioning, and the l is usually much smaller than m. Our goal is to recover the true signal $\mathbf{x}$ and detect $\mathbf{e}$ from the measurement $\mathbf{y}$, and we call it the outlier detection problem. The outlier detection problem has attracted the interests from different fields, such as system identification, channel coding and image and video processing [12–16]. For example, in the setting of channel coding, we consider a channel which can severely corrupt the signal the transmitter sends. The useful information is represented by $\mathbf{x}$ and is encoded by a transformation $\mathcal{M}$. When the encoded information goes through the channel, it is corrupted by gross errors introduced by the channel.

There exists a large volume of works on the outlier detection problem, ranging from the practical algorithms for recovering the true signal and detecting the outliers [12, 15–18], to recovery guarantees [9–12, 15, 16, 18, 19]. In [15], the channel decoding problem is considered and the authors proposed ℓ_1 minimization for outlier detection. By assuming $m > n$, Candes and Tao found an annihilator to transform the error correction problem into a basis pursuit problem, and established the theoretical recovery guarantees. Later in [16], Wright and Ma considered the same problem in a case where $m < n$. By assuming the true signal $\mathbf{x}$ is sparse, they reformulated the problem as an $\ell_1 \backslash \ell_1$ minimization. Based on a set of assumptions on the measuring matrix $\mathcal{M}$ and the sparse signals $\mathbf{x}$ and $\mathbf{e}$, they also established theoretical recovery guarantees. Xu et al. studied the sparse error correction problem with nonlinear measurements in [12], and proposed an iterative ℓ_1 minimization to detect outliers. By using a local linearization technique and an iterative ℓ_1 minimization algorithm, they showed that with high probability, the true signal could be recovered to high precision, and the iterative ℓ_1 minimization algorithm will converge to the true signal. All these algorithms and recovery guarantees are based on techniques from compressed sensing (CS), and usually they assume that the signal $\mathbf{x}$ is sparse over some basis, or generated from known physical models. In this paper, by applying techniques from deep learning, we will solve the outlier detection problem when $\mathbf{x}$ is generated from generative model in deep learning. We propose a generative model approach for solving outlier detection problem.

Deep learning [20] has attracted attentions from many fields in science and technology. Increasingly more researchers study the signal recovery problem from the deep learning prospective, such as implementing traditional signal recovery algorithms by deep neural networks [21–23], and providing recovery guarantees for nonconvex optimization approaches in deep learning [24–27]. In [24], the authors considered the case where the measurements are contaminated with Gaussian noise of small magnitude, and they proposed to use a generative model to recover the signal from noisy measurements.

Without requiring sparsity of the true signal, they showed that with high probability, the underlying signal can be recovered with small reconstruction error by ℓ_2 minimization. However, similar to traditional CS, the techniques presented in [24] can perform bad when the signal is corrupted with gross errors. Thus it is of interest to study the conditions under which the generative model can be applied to the outlier detection problems.

In this paper, we propose a framework for solving the outlier detection problem by using techniques from deep learning. Instead of finding directly $\mathbf{x} \in \mathbb{R}^n$ from its compressed measurement $\mathbf{y}$ under the sparsity assumption of $\mathbf{x}$, we will find a signal $\mathbf{z} \in \mathbb{R}^k$ which can be mapped into $\mathbf{x}$ or a small neighborhood of $\mathbf{x}$ by a generator $G(\cdot)$. The generator $G(\cdot)$ is implemented by a neural network, and examples include the variational auto-encoders or deep convolutional generative adversarial networks [24, 28, 29].

The generative-model-based approach is composed of two parts, i.e., the training process and the outlier detection process. In the former stage, by providing enough data samples $\{(\mathbf{z}^{(i)}, \mathbf{x}^{(i)})\}_{i=1}^N$, the generator will be trained to map $\mathbf{z}^{(i)} \in \mathbb{R}^k$ to $G(\mathbf{z}^{(i)})$ such that $G(\mathbf{z}^{(i)})$ can approximate $\mathbf{x}^{(i)} \in \mathbb{R}^n$ well. In the outlier detection stage, the well-trained generator will be combined with compressed sensing techniques to find a low-dimension representation $\mathbf{z} \in \mathbb{R}^k$ for $\mathbf{x} \in \mathbb{R}^n$, where the $(\mathbf{z}, \mathbf{x})$ can be outside the training dataset, but $\mathbf{z}$ and $\mathbf{x}$ has the same intrinsic relation as that between $\mathbf{z}^{(i)}$ and $\mathbf{x}^{(i)}$. In both of the two stages, we make no additional assumption on the structure of $\mathbf{x}$ and $\mathbf{z}$.

For our framework, we first give necessary and sufficient conditions under which the true signal can be recovered. We consider both the case where the generator is implemented by a linear neural network, and the case where the generator is implemented by a nonlinear neural network. In the linear neural network case, the generator is implemented by a d-layer neural network with random weight matrices $W^{(i)}$ and identity activation functions in each layer. We show that, when the ground true weight matrices $W^{(i)}$ of the generator are random matrices and the generator has already been well-trained, then with high probability, we can theoretically guarantee successful recovery of the ground truth signal under sparse outliers via ℓ_0 minimization. Our results are also applicable to the nonlinear neural networks.

We further propose an iterative alternating direction method of multipliers algorithm and gradient descent algorithm for the outlier detection. Our results show that our algorithm can outperform both the traditional Lasso and ℓ_2 minimization approach.

We summarize our contributions in this paper as follows:

- We propose a generative model based approach for the outlier detection, which further connects compressed sensing and deep learning.

- We establish the recovery guarantees for the proposed approach, which hold for generators implemented in linear or nonlinear neural networks. Our analytical techniques also hold for deep neural networks with arbitrary depth.

- Finally, we propose an iterative alternating direction method of multipliers algorithm for solving the outlier detection problem via ℓ_1 minimization, and a gradient descent algorithm for solving the same problem via squared ℓ_1 minimization. We

conduct extensive experiments to validate our theoretical analysis. Our algorithm can be of independent interest in solving nonlinear inverse problems.

The rest of the paper is organized as follows. In Section 2, we give a formal statement of the outlier detection problem, and give an overview of the framework of the generative-model approach. In Section 3, we propose the iterative alternating direction method of multipliers algorithm and the gradient descent algorithm. We present the recovery guarantees for generators implemented by both the linear and nonlinear neural networks in Section 4. Experimental results are presented in Section 5. We conclude this paper in Section 6.

Notations: In this paper, we will denote the ℓ_1 norm of an vector $\mathbf{x} \in \mathbf{R}^n$ by $\|\mathbf{x}\|_1 = \sum_{i=1}^{n} |\mathbf{x}_i|$, and the number of nonzero elements of an vector $\mathbf{x} \in \mathbf{R}^n$ by $\|\mathbf{x}\|_0$. For an vector $\mathbf{x} \in \mathbf{R}^n$ and an index set K with cardinality $|K|$, we let $(\mathbf{x})_K \in \mathbf{R}^{|K|}$ denote the vector consisting of elements from $\mathbf{x}$ whose indices are in K, and we let $(x)_{\bar{K}}$ denote the vector with all the elements from $\mathbf{x}$ whose indices are not in K. We denote the signature of a permutation σ by $\mathrm{sign}(\sigma)$. The value of $\mathrm{sign}(\sigma)$ is 1 or -1. The probability of an event $\mathcal{E}$ is denoted by $\mathbb{P}(\mathcal{E})$.

2 Problem Statement

In this section, we will model the outlier detection problem from the deep learning prospective, and introduce the necessary background needed for us to develop the method based on generative model.

Let generative model $G(\cdot) : \mathbb{R}^k \to \mathbb{R}^n$ be implemented by a d-layer neural network, and a conceptual diagram for illustrating the generator G is given in Fig. 1.

Define the bias terms in each layer as

$$\mathbf{b}^{(1)} \in \mathbb{R}^{n_1}, \mathbf{b}^{(2)} \in \mathbb{R}^{n_2}, \cdots, \mathbf{b}^{(d-1)} \in \mathbb{R}^{n_{d-1}}, \mathbf{b}^{(d)} \in \mathbb{R}^n.$$

Define the weight matrix $W^{(i)}$ in the i-th layer as

$$W^{(1)} = [w_1^{(1)}, w_2^{(1)}, \cdots, w_{n_1}^{(1)}]^T \in \mathbb{R}^{n_1 \times k}, w_j^{(1)} \in \mathbb{R}^k, j = 1, \cdots, n_1, \qquad (2.1)$$

$$W^{(i)} = [w_1^{(i)}, w_2^{(i)}, \cdots, w_{n_i}^{(i)}]^T \in \mathbb{R}^{n_i \times n_{i-1}}, w_j^{(i)} \in \mathbb{R}^{n_{i-1}}, 1 < i < d, j = 1 \cdots, n_i, \qquad (2.2)$$

and

$$W^{(d)} = [w_1^{(d)}, w_2^{(d)}, \cdots, w_n^{(d)}]^T \in \mathbb{R}^{n \times n_{d-1}}, w_j^{(d)} \in \mathbb{R}^{n_{d-1}}, j = 1, \cdots, n. \qquad (2.3)$$

The element-wise activation functions $a(\cdot)$ in different layers are defined to be the same, and some commonly used activation functions include the identity activation function, i.e.,
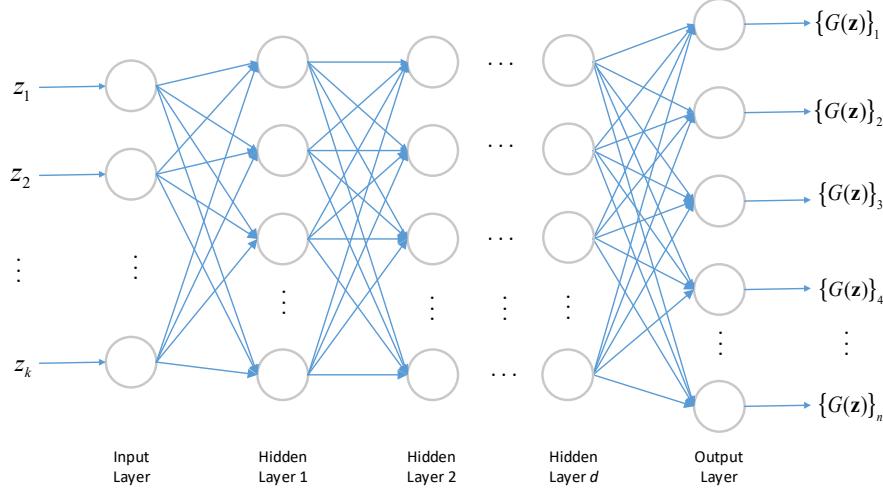
$$[a(x)]_i = x_i,$$

4

Figure 1: General Neural Network Structure of Generator

ReLU, i.e.,

$$[a(\mathbf{x})]_i = \begin{cases} 0, \text{if } \mathbf{x}_i < 0, \\ \mathbf{x}_i, \text{if } \mathbf{x}_i \geq 0, \end{cases} \tag{2.4}$$

and the leaky ReLU, i.e.,

$$[a(\mathbf{x})]_i = \begin{cases} \mathbf{x}_i, \text{if } \mathbf{x}_i \geq 0, \\ h\mathbf{x}_i, \text{if } \mathbf{x}_i < 0, \end{cases} \tag{2.5}$$

where $h \in (0,1)$ is a constant. Now for a given input $\mathbf{z} \in \mathbb{R}^k$, the output will be

$$G(\mathbf{z}) = a\left(W^{(d)}a\left(W^{(d-1)}\cdots a\left(W^{(1)}\mathbf{z} + \mathbf{b}^{(1)}\right)\cdots + \mathbf{b}^{(d-1)}\right) + \mathbf{b}^{(d)}\right). \tag{2.6}$$

Given the measurement vector $y \in \mathbb{R}^m$, i.e.,

$$\mathbf{y} = \mathcal{M}\mathbf{x} + \mathbf{e},$$

where the $\mathcal{M} \in \mathbb{R}^{m \times n}$ is a measurement matrix, $\mathbf{x}$ is a signal to be recovered, and the $\mathbf{e}$ is an outlier vector due to the corruption of measurement process. The $\mathbf{e}$ and $\mathbf{x}$ can be recovered via the following ℓ_0 "norm" minimization if $\mathbf{x}$ lies within the range of G, i.e.,

$$\min_{\mathbf{z} \in \mathbb{R}^k} \|\mathcal{M}G(\mathbf{z}) - \mathbf{y}\|_0.$$

However, the aforementioned ℓ_0 "norm" minimization is NP hard, thus we relax it to the following ℓ_1 minimization for recovering $\mathbf{x}$, i.e.,

$$\min_{\mathbf{z} \in \mathbb{R}^k} \|\mathcal{M}G(\mathbf{z}) - \mathbf{y}\|_1,$$

where $G(\cdot)$ is a well-trained generator. When the generator is well-trained, it can map low-dimension signal $\mathbf{z} \in \mathbb{R}^k$ to high-dimension signal $G(\mathbf{z}) \in \mathbb{R}^n$, and the $G(\mathbf{z})$ can well characterize the space $\mathbb{R}^n$. These well-trained generators will be used to solve the outlier detection problem, and we give a conceptual flowchart of the outlier detection stage in Fig. 2. Given a truth signal $\mathbf{x} \in \mathbf{R}^n$, we can get the compressed measurements $\mathbf{y} \in \mathbb{R}^m$ defined in (1.1) from $\mathbf{x}$. The goal is finding a $\mathbf{z} \in \mathbf{R}^k$ which can be mapped into $\hat{\mathbf{x}} = G(\mathbf{z}) \in \mathbf{R}^n$ satisfying the following property: when $\hat{\mathbf{x}}$ goes through the same measuring scheme, i.e., $\mathcal{M}$, the measurement $\hat{\mathbf{y}} \in \mathbf{R}^m$ will be close to the measurement $\mathbf{y}$ from the truth signal $\mathbf{x}$. Note that in Fig. 2, we do not include the training process. We further propose to solve the above ℓ_1 minimization by alternating direction method of multipliers (ADMM) algorithm which is introduced in Section 3. We also propose to solve the outlier detection problem by a gradient descent algorithm via a squared ℓ_1 minimization, i.e.,

$$\min_{\mathbf{z} \in \mathbb{R}^k} \|\mathcal{M}G(\mathbf{z}) - \mathbf{y}\|_1^2.$$

Remarks: In analysis, we focus on recovering signal and detecting outliers. However, our experimental results consider the signal recovery problem with the presence of both outliers and noise.
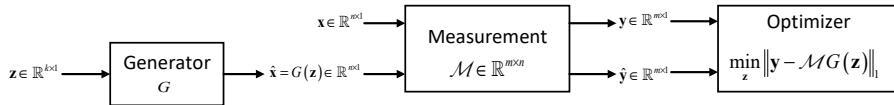

Figure 2: Deep Learning Based Compressed sensing system

Note that in [25], the authors considered the following problem

$$\min_{\mathbf{z},\mathbf{v}} \|\mathbf{e}\|_0$$
$$\text{s.t. } \mathcal{M}(G(\mathbf{z}) + \mathbf{e}) = \mathbf{y}.$$

Our problem is fundamentally different from the above problem. On the one hand, although the problem in [25] can also be treated as an outlier detection problem, the outlier occurs in signal $\mathbf{x}$ itself. However, in our problem, the outliers appear in the measuring process. On the other hand, our recovery performance guarantees are very different, and so are our analytical techniques.

3 Solving ℓ_1 Minimization via Gradient Descent and Alternating Direction Method of Multipliers

In this section, we introduce both gradient descent algorithm and alternating direction method of multipliers (ADMM) algorithm to solve the outlier detection problem.

We consider the ℓ_1 minimization in Section 2, i.e.,

$$\min_{\mathbf{z}\in\mathbb{R}^k} \|\mathcal{M}G(\mathbf{z}) - \mathbf{y}\|_1, \tag{3.1}$$

where $G(\cdot)$ is a well trained generator. Note that there can be different models for solving the outlier detection problem. We consider solving other problem models with different methods. For ℓ_1 minimization, we consider both the case where we solve

$$\min_{\mathbf{z}\in\mathbb{R}^k} \|\mathcal{M}G(\mathbf{z}) - \mathbf{y}\|_1 \tag{3.2}$$

by the ADMM algorithm introduced, and the case where we solve

$$\min_{\mathbf{z}\in\mathbb{R}^k} \|\mathcal{M}G(\mathbf{z}) - \mathbf{y}\|_1^2 \tag{3.3}$$

by the gradient descent (GD) algorithm [30]. For ℓ_2 minimization, we solve the following optimization problems:

$$\min_{\mathbf{z}\in\mathbb{R}^k} \|\mathcal{M}G(\mathbf{z}) - \mathbf{y}\|_2^2, \tag{3.4}$$

and

$$\min_{\mathbf{z}\in\mathbb{R}^k} \|\mathcal{M}G(\mathbf{z}) - \mathbf{y}\|_2^2 + \lambda\|\mathbf{z}\|_2^2. \tag{3.5}$$

Both the above two ℓ_2 norm minimizations are solved by gradient descent solver [30].

3.1 Gradient Descent Algorithm

Theoretically speaking, due to the non-differentiability of the ℓ_1 norm at 0, the gradient descent method cannot be applied to solve the problem (3.1). Our numerical experiments also show that direct GD for ℓ_1 norm does not yield good reconstruction results. However, once we turn to solve an equivalent problem, i.e.,

$$\min_{\mathbf{z}\in\mathbb{R}^k} \|\mathcal{M}G(\mathbf{z}) - \mathbf{y}\|_1^2, \tag{3.6}$$

the gradient descent algorithm can solve (3.6) in practice though ℓ_1 norm is not differentiable. Please see Section 5 for experimental results.

3.2 Iterative Linearized Alternating Direction Method of Multipliers Algorithm

Due to lack of theoretical guarantees, we propose an iterative linearized ADMM algorithm for solving (3.1) where the nonlinear mapping $G(\cdot)$ at each iteration is approximated via a linearization technique. Specifically, we introduce an auxiliary variable $\mathbf{w}$, and the above problem can be re-written as

$$\min_{\mathbf{z}\in\mathbb{R}^k,\mathbf{w}\in\mathbb{R}^m} \|\mathbf{w}\|_1$$
$$\text{s.t. } \mathcal{M}G(\mathbf{z}) - \mathbf{w} = \mathbf{y}. \tag{3.7}$$

The Augmented Lagrangian of (3.7) is given as

$$L_\rho(\mathbf{z}, \mathbf{w}, \lambda) = \|w\|_1 + \lambda^T(\mathcal{M}G(\mathbf{z}) - \mathbf{w} - \mathbf{y}) + \frac{\rho}{2}\|\mathcal{M}G(\mathbf{z}) - \mathbf{w} - \mathbf{y}\|_2^2,$$

or

$$L_\rho(\mathbf{z}, \mathbf{w}, \lambda) = \|\mathbf{w}\|_1 + \frac{\rho}{2}\left\|\mathcal{M}G(\mathbf{z}) - \mathbf{w} - \mathbf{y} + \frac{\lambda}{\rho}\right\|_2^2 - \frac{\rho}{2}\|\lambda/\rho\|_2^2,$$

where $\lambda \in \mathbb{R}^m$ and $\rho \in \mathbb{R}$ are Lagrangian multipliers and penalty parameter respectively. The main idea of ADMM algorithm is to update $\mathbf{z}$ and $\mathbf{w}$ alternatively. Notice that for both $\mathbf{w}$ and λ, they can be updated following the standard procedures. The nonlinearity and the lack of explicit form of the generator make it nontrivial to find the updating rule for $\mathbf{z}$. Here we consider a local linearization technique to solve the problem.

Consider the q-th iteration for $\mathbf{z}$, we have

$$\mathbf{z}^{q+1} = \arg\min_{\mathbf{z}} L_\rho\left(\mathbf{z}, \mathbf{w}^q, \lambda^q\right)$$
$$= \arg\min_{\mathbf{z}} F(\mathbf{z}), \tag{3.8}$$

where $F(\mathbf{z})$ is defined as

$$F(\mathbf{z}) = \left\|\mathcal{M}G(\mathbf{z}) - \mathbf{w}^q - \mathbf{y} + \frac{\lambda^q}{\rho}\right\|_2^2.$$

As we mentioned above, since $G(\mathbf{z})$ is non-linear, we will use a first order approximation, i.e.,

$$G(\mathbf{z}) \approx G(\mathbf{z}^q) + \nabla G(\mathbf{z}^q)^T(\mathbf{z} - \mathbf{z}^q), \tag{3.9}$$

where $\nabla G(\mathbf{z}^q)^T$ is the transpose of the gradient at $\mathbf{z}^q$. Then $F(\mathbf{z})$ will be

$$F(\mathbf{z}) = \left\|\mathcal{M}\left(G(\mathbf{z}^q) + \nabla G(\mathbf{z}^q)^T(\mathbf{z} - \mathbf{z}^q)\right) - \mathbf{w}^q - \mathbf{y} + \frac{\lambda^q}{\rho}\right\|_2^2$$
$$= \left\|\mathcal{M}\nabla G(\mathbf{z}^q)^T\mathbf{z} + \mathcal{M}\left(G(\mathbf{z}^q) - \nabla G(\mathbf{z}^q)^T\mathbf{z}^q\right) - \mathbf{w}^q - \mathbf{y} + \frac{\lambda^q}{\rho}\right\|_2^2. \tag{3.10}$$

The considered problem is a least square problem, and the minimum is achieved at

$$\mathbf{z}^{q+1} = (\mathcal{M}\nabla G(\mathbf{z}^q)^T)^\dagger \left(\mathbf{w}^q + \mathbf{y} - \frac{\lambda^q}{\rho} - \left(\mathcal{M}G(\mathbf{z}^q) - \mathcal{M}\nabla G(\mathbf{z}^q)^T \mathbf{z}^q \right) \right),$$

where $\dagger$ denotes the pseudo-inverse. Notice that both $\nabla G(\mathbf{z}^q)$ and $G(\mathbf{z}^q)$ will be automatically computed by the Tensorflow [31]. Similarly, we can update $\mathbf{w}$ and λ by

$$\mathbf{w}^{q+1} = \arg \min_{\mathbf{w}} \frac{\rho}{2} \left\| \mathcal{M}G\left(\mathbf{z}\right) - \mathbf{w}^q - \mathbf{y} + \frac{\lambda^q}{\rho} \right\|_2^2 + \|\mathbf{w}\|_1$$

$$= T_{\frac{1}{\rho}} \left(\mathcal{M}G\left(\mathbf{z}^{q+1}\right) - \mathbf{y} + \frac{\lambda^q}{\rho} \right), \tag{3.11}$$

and

$$\lambda^{q+1} = \lambda^q + \rho \left(\mathcal{M}G\left(\mathbf{z}^{q+1}\right) - \mathbf{w}^{q+1} - \mathbf{y} \right), \tag{3.12}$$

where $T_{\frac{1}{\rho}}$ is the element-wise soft-thresholding operator with parameter $\frac{1}{\rho}$ [32], i.e.,

$$[T_{\frac{1}{\rho}}(\mathbf{x})]_i = \begin{cases} [\mathbf{x}]_i - \frac{1}{\rho}, [\mathbf{x}]_i > \frac{1}{\rho}, \\ 0, |[\mathbf{x}]_i| \le \frac{1}{\rho}, \\ [\mathbf{x}]_i + \frac{1}{\rho}, [\mathbf{x}]_i < -\frac{1}{\rho}. \end{cases}$$

We continue ADMM algorithm to update $\mathbf{z}$ until optimization problem converges or stopping criteria are met. More discussion on stopping criteria and parameter tuning can be found in [32]. Our algorithm is summarized in Algorithm 1. The final value $\mathbf{z}^*$ can be used to generate the estimate $\hat{\mathbf{x}} = G(\mathbf{z}^*)$ for the true signal. We define the following metrics for evaluation: the measured error caused by imperfectness of CS measurement, i.e.,

$$\varepsilon_m \triangleq \|\mathbf{y} - \mathcal{M}G\left(\hat{\mathbf{z}}\right)\|_1, \tag{3.13}$$

and reconstructed error via a mismatch of $G(\hat{\mathbf{z}})$ and x, i.e.,

$$\varepsilon_r \triangleq \|\mathbf{x} - G\left(\hat{\mathbf{z}}\right)\|_2^2. \tag{3.14}$$

4 Performance Analysis

In this section, we present theoretical analysis of the performance of signal reconstruction method based on the generative model. We first establish the necessary and sufficient conditions for recovery in Theorems 4.1 and 4.2. Note that these two theorems appeared in [12], and we present them and their proofs here for the sake of completeness. We then show that both the linear and nonlinear neural network with an arbitrary number of layers can satisfy the recovery condition, thus ensuring successful reconstruction of signals.

9

Algorithm 1 Linearized ADMM

Input: $\mathbf{z}^0, \mathbf{w}^0, \lambda^0, \mathcal{M}$
Parameters: $\rho, MaxIte$
$q \leftarrow 0$
while $q \leq MaxIte$ **do**
    $A^{q+1} \leftarrow \mathcal{M}\nabla G(\mathbf{z}^q)^T$
    $\mathbf{z}^{q+1} \leftarrow (A^{q+1})^\dagger (\mathbf{w}^q + \mathbf{y} - \lambda^q/\rho - (\mathcal{M}G(\mathbf{z}^q) - A^{q+1}\mathbf{z}^q))$
    $\mathbf{w}^{q+1} \leftarrow T_{\frac{1}{\rho}} \left(\mathcal{M}G(\mathbf{z}^{q+1}) - \mathbf{y} + \frac{\lambda^q}{\rho} \right)$
    $\lambda^{q+1} \leftarrow \lambda^q + \rho(\mathcal{M}G(\mathbf{z}^{q+1}) - \mathbf{w}^{q+1} - \mathbf{y})$
end while
Output: $z^{MaxIte+1}$

4.1 Necessary and Sufficient Recovery Conditions

Suppose the ground truth signal $\mathbf{x}_0 \in \mathbb{R}^n$, the measurement matrix $\mathcal{M} \in \mathbb{R}^{m \times n} (m < n)$, and the sparse outlier vector $\mathbf{e} \in \mathbb{R}^m$ such that $\|\mathbf{e}\|_0 \leq l < m$, then the problem can be stated as

$$\min_{z \in \mathbb{R}^k} \|\mathcal{M}G(\mathbf{z}) - \mathbf{y}\|_0 \qquad (4.1)$$

where $\mathbf{y} = \mathcal{M}\mathbf{x}_0 + \mathbf{e}$ is a measurement vector and $G(\cdot) : \mathbb{R}^k \to \mathbb{R}^n$ is a generative model. Let $\mathbf{z}_0 \in \mathbb{R}^k$ be a vector such that $G(\mathbf{z}_0) = \mathbf{x}_0$, then we have following conditions under which the $\mathbf{z}_0$ can be recovered exactly without any sparsity assumption on neither $\mathbf{z}_0$ nor $\mathbf{x}_0$.

Theorem 4.1. *Let $G(\cdot), \mathbf{x}_0, \mathbf{z}_0, \mathbf{e}$ and $\mathbf{y}$ be as above. The vector $\mathbf{z}_0$ can be recovered exactly from (4.1) for any $\mathbf{e}$ with $\|\mathbf{e}\|_0 \leq l$ if and only if $\|\mathcal{M}G(\mathbf{z}) - \mathcal{M}G(\mathbf{z}_0)\|_0 \geq 2l+1$ holds for any $\mathbf{z} \neq \mathbf{z}_0$.*

Proof: We first show the sufficiency. Assume $\|\mathcal{M}G(\mathbf{z}) - \mathcal{M}G(\mathbf{z}_0)\|_0 \geq 2l+1$ holds for any $\mathbf{z} \neq \mathbf{z}_0$, since the triangle inequality gives

$$\|\mathcal{M}G(\mathbf{z}) - \mathcal{M}G(\mathbf{z}_0)\|_0 \leq \|\mathcal{M}G(\mathbf{z}_0) - \mathbf{y}\|_0 + \|\mathcal{M}G(\mathbf{z}) - \mathbf{y}\|_0,$$

then

$$\begin{aligned}
\|\mathcal{M}G(\mathbf{z}) - \mathbf{y}\|_0 &\geq \|\mathcal{M}G(\mathbf{z}) - \mathcal{M}G(\mathbf{z}_0)\|_0 - \|\mathcal{M}G(\mathbf{z}_0) - \mathbf{y}\|_0 \\
&= (2l+1) - l \\
&\geq l+1 \\
&> \|\mathcal{M}G(\mathbf{z}_0) - \mathbf{y}\|_0,
\end{aligned}$$

and this means $\mathbf{z}_0$ is a unique optimal solution to (4.1).

Next, we show the necessity by contradiction. Assume $\|\mathcal{M}G(\mathbf{z}) - \mathcal{M}G(\mathbf{z}_0)\|_0 \leq 2l$ holds for certain $\mathbf{z} \neq \mathbf{z}_0 \in \mathbb{R}^k$, and this means $\mathcal{M}G(\mathbf{z})$ and $\mathcal{M}G(\mathbf{z}_0)$ differ from each other over at most $2l$ entries. Denote by $\mathcal{I}$ the index set where $\mathcal{M}G(\mathbf{z}) - \mathcal{M}G(\mathbf{z}_0)$

has nonzero entries, then $|\mathcal{I}| \leq 2l$. We can choose outlier vector $\mathbf{e}$ such that $\mathbf{e}_i = (\mathcal{M}G(\mathbf{z}) - \mathcal{M}G(\mathbf{z}_0))_i$ for all $i \in \mathcal{I}' \subset \mathcal{I}$ with $|\mathcal{I}'| = l$, and $\mathbf{e}_i = 0$ otherwise. Then

$$\|\mathcal{M}G(\mathbf{z}) - \mathbf{y}\|_0 = \|\mathcal{M}G(\mathbf{z}) - \mathcal{M}G(\mathbf{z}_0) - \mathbf{e}\|_0 \leq 2l - l = l = \|\mathcal{M}G(\mathbf{z}_0) - \mathbf{y}\|_0, \tag{4.2}$$

which means we find an optimal solution $\mathbf{z}$ to (4.1) which is not $\mathbf{z}_0$. This contradicts the assumption.

$\square$

Theorem 4.1 gives a necessary and sufficient condition for successful recovery via ℓ_0 minimization, and we also present an equivalent condition as stated in Theorem 4.2 for successful recovery via ℓ_1 minimization.

Theorem 4.2. *Let* $G(\cdot), \mathbf{x}_0, \mathbf{z}_0, \mathbf{e}, \mathcal{M}$, *and* $\mathbf{y}$ *be the same as in Theorem 4.1. The low dimensional vector* $\mathbf{z}_0$ *can be recovered correctly from any* $\mathbf{e}$ *with* $\|\mathbf{e}\|_0 \leq l$ *from*

$$\min_{\mathbf{z}} \quad \|\mathbf{y} - \mathcal{M}G(\mathbf{z})\|_1, \tag{4.3}$$

if and only if for any $\mathbf{z} \neq \mathbf{z}_0$,

$$\|(\mathcal{M}G(\mathbf{z}_0) - \mathcal{M}G(\mathbf{z}))_K\|_1 < \|(\mathcal{M}G(\mathbf{z}_0) - \mathcal{M}G(\mathbf{z}))_{\overline{K}}\|_1,$$

where K *is the support of the error vector* $\mathbf{e}$.

Proof: We first show the sufficiency, i.e., if the $\|(\mathcal{M}G(\mathbf{z}_0) - \mathcal{M}G(\mathbf{z}))_K\|_1 < \|(\mathcal{M}G(\mathbf{z}_0) - \mathcal{M}G(\mathbf{z}))_{\overline{K}}\|_1$ holds for any $\mathbf{z} \neq \mathbf{z}_0$ where K is the support of $\mathbf{e}$, then we can correctly recover $\mathbf{z}_0$ from (4.3). For a feasible solution $\mathbf{z}$ to (4.3) which differs from $\mathbf{z}_0$, we have

$$\begin{aligned}
\|\mathbf{y} - \mathcal{M}G(\mathbf{z})\|_1 &= \|(\mathcal{M}G(\mathbf{z}_0) + \mathbf{e}) - \mathcal{M}G(\mathbf{z})\|_1 \\
&= \|\mathbf{e}_K - (\mathcal{M}G(\mathbf{z}) - \mathcal{M}G(\mathbf{z}_0))_K\|_1 + \|(\mathcal{M}G(\mathbf{z}) - \mathcal{M}G(\mathbf{z}_0))_{\overline{K}}\|_1 \\
&\geq \|\mathbf{e}_K\|_1 - \|(\mathcal{M}G(\mathbf{z}) - \mathcal{M}G(\mathbf{z}_0))_K\|_1 + \|(\mathcal{M}G(\mathbf{z}) - \mathcal{M}G(\mathbf{z}_0))_{\overline{K}}\|_1 \\
&> \|\mathbf{e}_K\|_1 = \|\mathbf{y} - \mathcal{M}G(\mathbf{z}_0)\|_1,
\end{aligned}$$

which means that $\mathbf{z}_0$ is the unique optimal solution to (4.3) and can be exactly recovered by solving (4.3).

We now show the necessity by contradiction. Suppose that there exists an $\mathbf{z} \neq \mathbf{z}_0$ such that $\|(\mathcal{M}G(\mathbf{z}_0) - \mathcal{M}G(\mathbf{z}))_K\|_1 \geq \|(\mathcal{M}G(\mathbf{z}_0) - \mathcal{M}G(\mathbf{z}))_{\overline{K}}\|_1$ with K being the support of $\mathbf{e}$. Then we can pick $\mathbf{e}_i$ to be $(\mathcal{M}G(\mathbf{z}) - \mathcal{M}G(\mathbf{z}_0))_i$ if $i \in K$ and 0 if $i \in \overline{K}$. Then

$$\begin{aligned}
\|\mathbf{y} - \mathcal{M}G(\mathbf{z})\|_1 &= \|\mathcal{M}G(\mathbf{z}_0) - \mathcal{M}G(\mathbf{z}) + \mathbf{e}\|_1 \\
&= \|(\mathcal{M}G(\mathbf{z}) - \mathcal{M}G(\mathbf{z}_0))_{\overline{K}}\|_1 \\
&\leq \|(\mathcal{M}G(\mathbf{z}) - \mathcal{M}G(\mathbf{z}))_K\|_1 \\
&= \|\mathbf{e}\|_1 = \|y - \mathcal{M}G(\mathbf{z}_0)\|_1,
\end{aligned}$$

11

which means that $\mathbf{z}_0$ cannot be the unique optimal solution to (4.3). Thus

$$\|(\mathcal{M}G(\mathbf{z}) - \mathcal{M}G(\mathbf{z}_0))_{\overline{K}}\|_1 > \|(\mathcal{M}G(\mathbf{z}) - \mathcal{M}G(\mathbf{z}))_K\|_1$$

must holds for any $\mathbf{z} \neq \mathbf{z}_0$.

$\square$

4.2 Full Rankness of Random Matrices

Before we proceed to the main results, we give some technical lemmas which will be used to prove our main theorems.

Lemma 4.3. *([33]) Let $P \in A[X_1, \cdots, X_v]$ be a polynomial of total degree D over an integral domain A. Let $\mathfrak{J}$ be a subset of A of cardinality B. Then*

$$\mathbb{P}(P(x_1, \cdots, x_v) = 0 | x_i \in \mathfrak{J}) \leq \frac{D}{B}.$$

Lemma 4.3 gives an upper bound of the probability for a polynomial to be zero when its variables are randomly taken from a set. Note that in [34], the authors applied the Lemma 4.3 to study the adjacency matrix from an expander graph. Since the determinant of a square random matrix is a polynomial, Lemma 4.3 can be applied to determine whether a square random matrix is rank deficient. An immediate result will be Lemma 4.4.

Lemma 4.4. *A random matrix $M \in \mathbb{R}^{m \times n}$ with independent Gaussian entries will have full rank with probability 1, i.e., $\mathrm{rank}(M) = \min(m, n)$.*

*P*roof: For simplicity of presentation, we consider the square matrix case, i.e., a random matrix $M \in \mathbb{R}^{n \times n}$ whose entries are drawn i.i.d. randomly from $\mathbb{R}$ according to standard Gaussian distribution $\mathcal{N}(0, 1)$.

Note that

$$\det(M) = \sum_{\sigma} \left(\mathrm{sign}(\sigma) \prod_{i=1}^{n} M_{i\sigma(i)} \right)$$

where σ is a permutation of $\{1, 2, \cdots, n\}$, the summation is over all $n!$ permutations, and $\mathrm{sign}(\sigma)$ is either $+1$ or -1. Since $\det(M)$ is a polynomial of degree n with respect to $M_{ij} \in \mathbb{R}$, $i, j = 1, \cdots, n$ and the $\mathbb{R}$ has infinitely many elements, then according to Lemma 4.3, we have

$$\mathbb{P}(\det(M) = 0) \leq 0.$$

Thus

$$\mathbb{P}(M \text{ has full rank}) = \mathbb{P}(\det(M) \neq 0) \geq 1 - \mathbb{P}(\det(M) = 0),$$

and this means the Gaussian random matrix has full rank with probability 1.

$\square$

Remarks: (1) We can easily extend the arguments to random matrix with arbitrary shape, i.e., $M \in \mathbb{R}^{m \times n}$. Considering arbitrary square sub-matrix with size $\min(m,n) \times \min(m,n)$ from M, following the same arguments will give that with probability 1, the matrix M has full rank with $\text{rank}(M) = \min(m,n)$; (2) The arguments in Lemma 4.4 can also be extended to random matrix with other distributions.

4.3 Generative Models via Linear Neural Networks

We first consider the case where the activation function is an element-wise identity operator, i.e., $a(\mathbf{x}) = \mathbf{x}$, and this will give us a simplified input and output relation as follows

$$G(\mathbf{z}) = W^{(d)} W^{(d-1)} \cdots W^{(1)} \mathbf{z}. \qquad (4.4)$$

Define $W = W^{(d)} W^{(d-1)} \cdots W^{(1)}$, we get a simplified relation $G(\mathbf{z}) = W\mathbf{z}$. We will show that with high probability: for any $\mathbf{z} \neq \mathbf{z}_0$, the

$$\|G(\mathbf{z}) - G(\mathbf{z}_0)\|_0 = \|W(\mathbf{z} - \mathbf{z}_0)\|_0$$

will have at least $2l + 1$ nonzero entries; or when we treat the $\mathbf{z} - \mathbf{z}_0$ as a whole and still use the letter $\mathbf{z}$ to denote $\mathbf{z} - \mathbf{z}_0$, then for any $\mathbf{z} \neq 0$, the

$$\mathbf{v} := W\mathbf{z}$$

will have at least $2l + 1$ nonzero entries.

Note that in the above derivation, the bias term is incorporated in the weight matrix. For example, in the first layer, we know

$$W^{(1)} \mathbf{z} + \mathbf{b}^{(1)} = [W^{(1)} \ \mathbf{b}^{(1)}] \begin{bmatrix} \mathbf{z} \\ 1 \end{bmatrix}.$$

Actually, when the $W^{(i)}$ does not incorporate the bias term $\mathbf{b}^{(i)}$, we have a generator as follows

$$
\begin{aligned}
G(z) &= W^{(d)} \left(W^{(d-1)} \left(\cdots \left(W^{(2)} \left(W^{(1)} \mathbf{z} + \mathbf{b}^{(1)} \right) + \mathbf{b}^{(2)} \right) \right) + \cdots + \mathbf{b}^{(d-1)} \right) + \mathbf{b}^{(d)} \\
&= W^{(d)} \cdots W^{(1)} \mathbf{z} + W^{(d)} \cdots W^{(2)} \mathbf{b}^{(1)} + W^{(d)} \cdots W^{(3)} \mathbf{b}^{(2)} \\
&\quad + \cdots + W^{(d)} \mathbf{b}^{(d-1)} + \mathbf{b}^{(d)}.
\end{aligned}
$$

We can define $W = W^{(d)} \cdots W^{(1)}$. Then in this case, we need to show that with high probability: for any $\mathbf{z} \neq \mathbf{z}_0$, the

$$\|G(\mathbf{z}) - G(\mathbf{z}_0)\|_0 = \|W(\mathbf{z} - \mathbf{z}_0)\|_0$$

has at least $2l + 1$ nonzero entries because all the other terms are cancelled.

Lemma 4.5. *Let matrix $W \in \mathbb{R}^{n \times k}$. Then for an integer $l \geq 0$, if every $r := n - (2l + 1) \geq k$ rows of W has full rank k, then $\mathbf{v} = W\mathbf{z}$ can have at most $n - (2l + 1)$ zero entries for every $\mathbf{z} \neq 0 \in \mathbb{R}^k$.*

Proof: Suppose $\mathbf{v} = W\mathbf{z}$ has $n - (2l + 1) + 1$ zeros, we denote by $S_{\mathbf{v}}$ the set of indices where the corresponding entries of $\mathbf{v}$ are nonzero, and by $\bar{S}_{\mathbf{v}}$ the set of indices where the corresponding entries of $\mathbf{v}$ are zero, then $|\bar{S}_{\mathbf{v}}| = n - (2l + 1) + 1$. Then for the homogeneous linear equations

$$\mathbf{0} = \mathbf{v}_{\bar{S}_{\mathbf{v}}} = W_{\bar{S}_{\mathbf{v}}}\mathbf{z},$$

where $W_{\bar{S}_{\mathbf{v}}}$ consists of $|\bar{S}_{\mathbf{v}}| = n - (2l + 1) + 1$ rows from W with indices in $\bar{S}_{\mathbf{v}}$, the matrix $W_{\bar{S}_{\mathbf{v}}}$ must have a rank less than k so that there exists such a nonzero solution $\mathbf{z}$. Then there exists a sub-matrix consisting of $n - (2l + 1)$ rows which has rank less than k, and this contradicts the statement.

$\square$

The Lemma 4.5 actually gives a sufficient condition for $\mathbf{v} = W\mathbf{z}$ to have at least $2l + 1$ nonzero entries, i.e., every $n - (2l + 1)$ rows of W has full rank k.

Lemma 4.6. *Let the composite weight matrix in multiple-layer neural network with identity activation function be*

$$W = W^{(d)}W^{(d-1)} \cdots W^{(1)},$$

where

$$W^{(1)} = [w_1^{(1)}, w_2^{(1)}, \cdots, w_{n_1}^{(1)}]^T \in \mathbb{R}^{n_1 \times k}, w_j^{(1)} \in \mathbb{R}^k, j = 1, \cdots, n_1,$$

$$W^{(i)} = [w_1^{(i)}, w_2^{(i)}, \cdots, w_{n_i}^{(i)}]^T \in \mathbb{R}^{n_i \times n_{i-1}}, w_j^{(i)} \in \mathbb{R}^{n_{i-1}}, 1 < i < d, j = 1 \cdots, n_i,$$

and

$$W^{(d)} = [w_1^{(d)}, w_2^{(d)}, \cdots, w_n^{(d)}]^T \in \mathbb{R}^{n \times n_{d-1}}, w_j^{(d)} \in \mathbb{R}^{n_{d-1}}, j = 1, \cdots, n,$$

with $n_i \geq k, i = 1, \cdots, d - 1$ and $n > k$. When $d = 1$, we let $W = W^{(1)} \in \mathbb{R}^{n \times k}$. Let each entry in each weight matrix $W^{(i)}$ be drawn independently randomly according to the standard Gaussian distribution, $\mathcal{N}(0, 1)$. Then for a linear neural network of two or more layers with composite weight matrix W defined above, with probability 1, every $r = n - (2l + 1) \geq k$ rows of W will have full rank k.

Proof: We will show Lemma 4.6 by induction.

2-layer case: When there are only two layers in the neural network, we have

$$W = W^{(2)}W^{(1)}$$

where $W^{(1)} \in \mathbb{R}^{n_1 \times k}$ ($n_1 \geq k$) and $W^{(2)} \in \mathbb{R}^{n \times n_1}$ ($n \geq n_1$). From Lemma 4.4, with probability 1, the matrix $W^{(1)}$ has full rank and a singular value decomposition

$$W^{(1)} = U^{(1)}\Sigma^{(1)}(V^{(1)})^*,$$

where $\Sigma^{(1)} \in \mathbb{R}^{k \times k}$ and $V^{(1)} \in \mathbb{R}^{k \times k}$ have rank k, and $U^{(1)} \in \mathbb{R}^{n_1 \times k}$.

For the matrix $W^{(2)}W^{(1)}$, we take arbitrary $r = n - (2l + 1) \geq k$ rows of $W^{(2)}$ to form a new matrix $M^{(2)}$, and we have

$$l \leq \frac{n - 1 - k}{2},$$

and

$$M^{(2)}W^{(1)} = M^{(2)}U^{(1)}\Sigma^{(1)}(V^{(1)})^*.$$

Since $\Sigma^{(1)}$ and $V^{(1)}$ have full rank k, then

$$\mathrm{rank}(M^{(2)}W^{(1)}) = \mathrm{rank}(M^{(2)}U^{(1)}).$$

If we fix the matrix $W^{(1)}$, then $U^{(1)}$ will also be fixed. The matrix $M^{(2)}U^{(1)}$ has full rank k with probability 1, so is $M^{(2)}W^{(1)}$. Notice that we have totally $\binom{n}{n-(2l+1)}$ choices for forming $M^{(2)}$, thus according to the union bound, the probability for existence of a matrix $M^{(2)}$ which makes $M^{(2)}W^{(1)}$ rank deficient satisfies

$$\mathbb{P}(\text{there exist a matrix } M^{(2)} \text{ such that } M^{(2)}W^{(1)} \text{ is rank deficient}) \leq \binom{n}{n-(2l+1)} \times 0 = 0.$$

Thus, the probability for all such matrices $M^{(2)}$ to have full rank is 1.

$(d-1)$-**layer case:** Assume for the case with $d - 1$ layers, arbitrary $n - (2l + 1)$ rows of the weight matrix
$$W = W^{(d-1)}W^{(d-2)} \cdots W^{(1)}$$

will form a matrix with full rank k, where $W^{(d-1)} \in \mathbb{R}^{n \times n_{d-2}}$ and $W^{(d-2)} \in \mathbb{R}^{n_{d-2} \times n_{d-3}}$. Then for $W^{(d-2)} \cdots W^{(1)}$, it will have rank k and singular value decomposition
$$W^{(d-2)} \cdots W^{(1)} = U\Sigma V^*,$$

where $U \in \mathbb{R}^{n_{d-2} \times k}$, $\Sigma \in \mathbb{R}^{k \times k}$ and $V \in \mathbb{R}^{k \times k}$.

d-**layer case:** Now we consider the case with d layers. The corresponding composite weight matrix becomes

$$W = W^{(d)}W^{(d-1)}W^{(d-2)} \cdots W^{(1)}$$

where $W^{(d)} \in \mathbb{R}^{n \times n_{d-1}}$, $W^{(d-1)} \in \mathbb{R}^{n_{d-1} \times n_{d-2}}$ and $W^{(d-2)} \in \mathbb{R}^{n_{d-2} \times n_{d-3}}$.

Since
$$W^{(d-2)} \cdots W^{(1)} = U\Sigma V^*,$$

then

$$W = W^{(d)}W^{(d-1)}U\Sigma V^*.$$

Note that
$$\text{rank}(W^{(d-1)}U\Sigma V^*) = \text{rank}(W^{(d-1)}U),$$

$W^{(d-1)}U$ is a matrix of full rank k with probability 1 and has a singular value decomposition as
$$W^{(d-1)}U = \tilde{U}\tilde{\Sigma}\tilde{V}^*,$$

where $\tilde{U} \in \mathbb{R}^{n_{d-1}\times k}$, $\tilde{\Sigma} \in \mathbb{R}^{k\times k}$ and $\tilde{V} \in \mathbb{R}^{k\times k}$. Follow the similar arguments above, every $n - (2l + 1)$ rows of $W^{(d)}W^{(d-1)}W^{(d-2)}\cdots W^{(1)}$ will have full rank k.

$\square$

Remarks: Actually the statement also holds when $d = 1$. When the NN has only 1 layer, we have $W = W^{(1)}$. Then matrix $M^{(1)}$ consisting of arbitrary r rows in W will also be a random matrix with each entry drawn i.i.d. randomly according to Gaussian distribution, thus with probability 1, the matrix $M^{(1)}$ will have full rank k.

Thus, we can conclude that for every $\mathbf{z} \neq 0 \in \mathbb{R}^k$, if the weight matrices are defined as above, then the $y = Wx \in \mathbb{R}^n$ will have at least $2l + 1$ nonzero elements, and the successful recovery is guaranteed by the following theorem.

Theorem 4.7. *Let the generator $G(\cdot)$ be implemented by a multiple-layer neural network with identity activation function. The weight matrix in each layer is defined as*
$$W^{(1)} = [w_1^{(1)}, w_2^{(1)}, \cdots, w_{n_1}^{(1)}]^T \in \mathbb{R}^{n_1 \times k}, w_j^{(1)} \in \mathbb{R}^k, j = 1, \cdots, n_1$$

$$W^{(i)} = [w_1^{(i)}, w_2^{(i)}, \cdots, w_{n_i}^{(i)}]^T \in \mathbb{R}^{n_i \times n_{i-1}}, w_j^{(i)} \in \mathbb{R}^{n_{i-1}}, 1 < i < d, j = 1 \cdots, n_i,$$

and
$$W^{(d)} = [w_1^{(d)}, w_2^{(d)}, \cdots, w_n^{(d)}]^T \in \mathbb{R}^{n \times n_{d-1}}, w_j^{(d)} \in \mathbb{R}^{n_{d-1}}, j = 1, \cdots, n,$$

with $n_i \geq k, i = 1, \cdots, d - 1$ and $n > k$. Each entry in each weight matrix $W^{(i)}$ is independently randomly drawn from standard Gaussian distribution $\mathcal{N}(0, 1)$. Let the measurement matrix $\mathcal{M} \in \mathbb{R}^{m\times n}$ be a random matrix with each entry iid drawn according to standard Gaussian distribution $\mathcal{N}(0, 1)$. Let the true signal $\mathbf{x}_0$ and its corresponding low dimensional signal $\mathbf{z}_0$, the outlier signal $\mathbf{e}$ and $\mathbf{y}$ be the same as in Theorem 4.1 and satisfy
$$\|\mathbf{e}\|_0 \leq \frac{n-1-k}{2}.$$

Then with probability 1: for a well-trained generator $G(\cdot)$, every $\mathbf{z}_0$ can be recovered from
$$\min_{\mathbf{z}\in\mathbb{R}^k} \|\mathcal{M}G(\mathbf{z}) - y\|_0.$$

Proof: Notice that in this case, we have
$$\mathcal{M}G(\mathbf{z}) = \mathcal{M}W^{(d)}W^{(d-1)}\cdots W^{(1)}\mathbf{z}.$$

Since $\mathcal{M}^{m\times n}$ is also a random matrix with i.i.d. Gaussian entries $l \leq \frac{n-1-k}{2}$, we can actually treat $\mathcal{M}G(\mathbf{z})$ as a $(d + 1)$-layer neural network implementation of the

generator acting on $\mathbf{z}$. Then according to Lemma 4.6, every $m - (2l + 1)$ rows of $\mathcal{M}W^{(d)}W^{(d-1)}\cdots W^{(1)}$ will have full rank k. The Lemma 4.5 implies that the $\mathcal{M}W^{(d)}W^{(d-1)}\cdots W^{(1)}(\mathbf{z} - \mathbf{z}_0)$ can have at most $m - (2l + 1)$ zero entries for every $\mathbf{z} \neq \mathbf{z}_0$. Finally, from Theorem 4.1, the $\mathbf{z}_0$ can be recovered with probability 1.

$\square$

4.4 Generative Models via Nonlinear Neural Network

In previous sections, we have show that when the activation function $a(\cdot)$ is the identity function, we can show that with high probability, the generative model implemented via neural network can successfully recover the true signal $\mathbf{z}_0$. In this section, we will extend our analysis to the neural network with nonlinear activation functions.

Notice that in the proof of neural networks with identity activation, the key is that we can write $G(\mathbf{z}) - G(\mathbf{z}_0)$ as $W(\mathbf{z} - \mathbf{z}_0)$, which allows us to characterize the recovery conditions by the properties of linear equation systems. However, in neural network with nonlinear activation functions, we do not have such linear properties. For example, in the case of leaky ReLU activation function, i.e.,

$$[a(\mathbf{x})]_i = \begin{cases} \mathbf{x}_i, \mathbf{x}_i \geq 0, \\ h\mathbf{x}_i, \mathbf{x}_i < 0, \end{cases}$$

where $h \in (0, 1)$, for an $\mathbf{z} \neq \mathbf{z}_0$, the sign patterns of $\mathbf{z}$ and $\mathbf{z}_0$ can be different, and this results in that the rows of the weight matrix in each layer will be scaled by different values. Thus we cannot directly transform $G(\mathbf{z}) - G(\mathbf{z}_0)$ into $W(\mathbf{z} - \mathbf{z}_0)$. Fortunately, we can achieve the transformation via Lemma 4.8 for the leaky ReLU activation function.

Lemma 4.8. *Define the leaky ReLU activation function as*

$$a(x) = \begin{cases} x, x \geq 0, \\ hx, x < 0, \end{cases}$$

where $x \in \mathbb{R}$ and $h \in (0, 1)$, then for arbitrary $x \in \mathbb{R}$ and $y \in \mathbb{R}$, the $a(x) - a(y) = \beta(x - y)$ holds for some $\beta \in [h, 1]$ regardless of the sign patterns of x and y.

Proof: When x and y have the same sign pattern, i.e., $x \geq 0$ and $y \geq 0$ holds simultaneously, or $x < 0$ and $y < 0$ holds simultaneously, then

$$a(x) - a(y) = x - y,$$

with $\beta = 1$, or

$$a(x) - a(y) = hx - hy = h(x - y),$$

with $\beta = h \in (0, 1)$.

When x and y have different sign patterns, we have the following two cases: (1) $x \geq 0$ and $y < 0$ holds simultaneously; (2) $x < 0$ and $y \geq 0$ holds simultaneously. For the first case, we have

$$a(x) - a(y) = x - hy = \beta(x - y),$$

which gives

$$\beta = \frac{x - hy}{x - y} > \frac{hx - hy}{x - y} = h,$$

and

$$\beta = \frac{x - hy}{x - y} < \frac{x - y}{x - y} = 1,$$

where we use the facts that $x \geq 0$, $y < 0$ and $h \in (0, 1)$.

Thus $\beta \in (h, 1)$, and similarly for $x < 0$ and $y \geq 0$. Combine the above cases together, we have $\beta \in [h, 1]$.

$\square$

Since in the neural network, the leaky ReLU acts on the weighted sum $W\mathbf{z}$ element-wise, we can easily extend Lemma 4.8 to the high dimensional case. For example, consider the first layer with weight $W^{(1)} \in \mathbb{R}^{n_1 \times k}$, bias $\mathbf{b}^{(1)} \in \mathbb{R}^{n_1}$, and leaky ReLU activation function, we have

$$a^{(1)}(W^{(1)}\mathbf{z} + \mathbf{b}^{(1)}) - a^{(1)}(W^{(1)}\mathbf{z}_0 + \mathbf{b}^{(1)})$$

$$= \begin{bmatrix} \beta_1^{(1)}([W^{(1)}\mathbf{z} + \mathbf{b}^{(1)}]_1 - [W^{(1)}\mathbf{z}_0 + \mathbf{b}^{(1)}]_1) \\ \beta_2^{(1)}([W^{(1)}\mathbf{z} + \mathbf{b}^{(1)}]_2 - [W^{(1)}\mathbf{z}_0 + \mathbf{b}^{(1)}]_2) \\ \vdots \\ \beta_{n_1}^{(1)}([W^{(1)}\mathbf{z} + \mathbf{b}^{(1)}]_{n_1} - [W^{(1)}\mathbf{z}_0 + \mathbf{b}^{(1)}]_{n_1}) \end{bmatrix}$$

$$= \begin{bmatrix} \beta_1^{(1)} & 0 & \cdots & 0 \\ 0 & \beta_2^{(1)} & \cdots & 0 \\ \vdots & \vdots & \ddots & 0 \\ 0 & 0 & \cdots & \beta_{n_1}^{(1)} \end{bmatrix} ((W^{(1)}\mathbf{z} + \mathbf{b}^{(1)}) - (W^{(1)}\mathbf{z}_0 + \mathbf{b}^{(1)}))$$

$$= \Gamma^{(1)}W^{(1)}(\mathbf{z} - \mathbf{z}_0),$$

where $\beta_i^{(1)} \in [h, 1]$ for every $i = 1, \cdots, n_1$, and

$$\Gamma^{(1)} = \begin{bmatrix} \beta_1^{(1)} & 0 & \cdots & 0 \\ 0 & \beta_2^{(1)} & \cdots & 0 \\ \vdots & \vdots & \ddots & 0 \\ 0 & 0 & \cdots & \beta_{n_1}^{(1)} \end{bmatrix}.$$

Since $\Gamma^{(1)}$ has full rank, it does not affect the rank of $W^{(1)}$, and we can treat their product as a full rank matrix $P^{(1)} = \Gamma^{(1)}W^{(1)}$. In this way, we can apply the techniques in the linear neural networks to the one with leaky ReLU activation function.

Remarks: Note that even though the Lemma 4.8 applies to ReLU activation function with $\beta \in [0, 1]$, the Γ matrix we construct can be rank deficient, which can cause the results in the linear neural network to fail;

Lemma 4.9. *Let the generative model $G(\cdot) : \mathbb{R}^k \to \mathbb{R}^n$ be implemented by a d-layer neural network, i.e.,*

$$G(\mathbf{z}) = a^{(d)} \left(W^{(d)} a^{(d-1)} \left(W^{(d-1)} \cdots a^{(1)} \left(W^{(1)} \mathbf{z} + \mathbf{b}^{(1)} \right) \cdots + \mathbf{b}^{(d-1)} \right) + \mathbf{b}^{(d)} \right).$$

Let the weight matrix in each layer be defined as

$$W^{(1)} = [w_1^{(1)}, w_2^{(1)}, \cdots, w_{n_1}^{(1)}]^T \in \mathbb{R}^{n_1 \times k}, w_j^{(1)} \in \mathbb{R}^k, j = 1, \cdots, n_1,$$

$$W^{(i)} = [w_1^{(i)}, w_2^{(i)}, \cdots, w_{n_i}^{(i)}]^T \in \mathbb{R}^{n_i \times n_{i-1}}, w_j^{(i)} \in \mathbb{R}^{n_{i-1}}, 1 < i < d, j = 1, \cdots, n_i$$

and

$$W^{(d)} = [w_1^{(d)}, w_2^{(d)}, \cdots, w_n^{(d)}]^T \in \mathbb{R}^{n \times n_{d-1}}, w_j^{(d)}, j = 1, \cdots, n,$$

with

$$n_i \geq k, i = 1, \cdots, d - 1,$$

and

$$k \leq n - (2l + 1).$$

Let each entry in each weight matrix $W^{(i)}$ be drawn iid randomly according to the standard Gaussian distribution $\mathcal{N}(0, 1)$. Let the element-wise activation function $a^{(i)}$ in the i-th layer be a leaky ReLU, i.e.,

$$[a^{(i)}(x)]_j = \begin{cases} x_j, \text{ if } x_j \geq 0, \\ h^{(i)} x_j, \text{ if } x_j < 0, \end{cases} , i = 1, \cdots, d,$$

where $h^{(i)} \in (0, 1)$.

Then with high probability, the following holds: for every $\mathbf{z} \neq \mathbf{z}_0$,

$$\|G(\mathbf{z}_0) - G(\mathbf{z})\|_0 \geq 2l + 1,$$

where $G(\cdot)$ is the generative model defined above.

Proof: Apply the Lemma 4.8, we have

$$G(\mathbf{z}) = a^{(d)}\left(W^{(d)}a^{(d-1)}\left(W^{(d-1)}\cdots a^{(1)}\left(W^{(1)}\mathbf{z}\right)\right)\right)$$

$$= \begin{bmatrix} h_1^{(d)} & 0 & \cdots & 0 \\ 0 & h_2^{(d)} & \cdots & 0 \\ \vdots & \vdots & \ddots & \vdots \\ 0 & 0 & \cdots & h_n^{(d)} \end{bmatrix} W^{(d)} \begin{bmatrix} h_1^{(d-1)} & 0 & \cdots & 0 \\ 0 & h_2^{(d-1)} & \cdots & 0 \\ \vdots & \vdots & \ddots & \vdots \\ 0 & 0 & \cdots & h_{n_{d-1}}^{(d-1)} \end{bmatrix} W^{(d-1)}$$

$$\times \cdots \times \begin{bmatrix} h_1^{(1)} & 0 & \cdots & 0 \\ 0 & h_2^{(1)} & \cdots & 0 \\ \vdots & \vdots & \ddots & \vdots \\ 0 & 0 & \cdots & h_{n_1}^{(1)} \end{bmatrix} W^{(1)}\mathbf{z}$$

$$= \begin{bmatrix} h_1^{(d)}\left(w_1^{(d)}\right)^T \\ h_2^{(d)}\left(w_2^{(d)}\right)^T \\ \vdots \\ h_n^{(d)}\left(w_n^{(d)}\right)^T \end{bmatrix} \begin{bmatrix} h_1^{(d-1)}\left(w_1^{(d-1)}\right)^T \\ h_2^{(d-1)}\left(w_2^{(d-1)}\right)^T \\ \vdots \\ h_{n_{d-1}}^{(d-1)}\left(w_{n_{d-1}}^{(d-1)}\right)^T \end{bmatrix} \cdots \begin{bmatrix} h_1^{(1)}\left(w_1^{(1)}\right)^T \\ h_2^{(1)}\left(w_2^{(1)}\right)^T \\ \vdots \\ h_{n_1}^{(1)}\left(w_{n_1}^{(1)}\right)^T \end{bmatrix} \mathbf{z},$$

where $h_j^{(i)} \in [h, 1]$.

Denote the scaled matrix by

$$P^{(1)} = \begin{bmatrix} h_1^{(1)}\left(w_1^{(1)}\right)^T \\ h_2^{(1)}\left(w_2^{(1)}\right)^T \\ \vdots \\ h_{n_1}^{(1)}\left(w_{n_1}^{(d)}\right)^T \end{bmatrix}, \cdots, P^{(d)} = \begin{bmatrix} h_1^{(d)}\left(w_1^{(d)}\right)^T \\ h_2^{(d)}\left(w_2^{(d)}\right)^T \\ \vdots \\ h_n^{(d)}\left(w_n^{(d)}\right)^T \end{bmatrix},$$

then we know that $P^{(i)}, i = 1, \cdots, d$ have independent Gaussian entries and the generative model becomes

$$G(\mathbf{z}) = P^{(d)}P^{(d-1)}\cdots P^{(1)}\mathbf{z}. \tag{4.5}$$

From Lemma 4.5, we only need to show that every $r = n - (2l + 1)$ rows of $P^{(d)}P^{(d-1)}\cdots P^{(1)}$ have full rank k. Following the arguments in proving Lemma 4.6, we can show that every $r = n - (2l + 1)$ rows of $P^{(d)}P^{(d-1)}\cdots P^{(1)}$ has full rank k. Thus we can arrive at our conclusion.

$\square$

Now we can get the recovery guarantee for generator implemented by arbitrary layer neural network with leaky ReLU activation functions as stated in Theorem 4.10.

Theorem 4.10. *Let the generator $G(\cdot)$ be implemented by a neural network described in Lemma 4.9. Let the true signal $\mathbf{x}_0$ and its corresponding low dimensional signal $\mathbf{z}_0$, the outlier signal $\mathbf{e}$ and observation $\mathbf{y}$ be the same as in Theorem 4.1. Let the measurement matrix $\mathcal{M} \in \mathbb{R}^{m \times n}$ be a random matrix with all entries iid random according to the Gaussian distribution and $\min(m, n) > l$. Then with high probability, the $\mathbf{z}_0$ can be recovered by solving*

$$\min_{\mathbf{z} \in \mathbb{R}^n} \|\mathcal{M}G(\mathbf{z}) - \mathbf{y}\|_0.$$

Proof: Following the argument in Lemma 4.9, we have

$$\mathcal{M}G(\mathbf{z}) = \mathcal{M}P^{(d)}P^{(d-1)} \cdots P^{(1)}\mathbf{z}.$$

Similar to the case where the generator is implemented by a linear neural network, the matrix $\mathcal{M}$ can be treated as the weight matrix in the $(d+1)$-th layer, and $P^{(i)}$ is the weight matrix in the i-th layer, and the activation functions are identity maps. Then according to Lemma 4.6, every $n - (2l+1)$ rows of $P = P^{(d)}P^{(d-1)} \cdots P^{(1)}$ will have full rank k, and Lemma 4.5 implies that the $P(z - z_0)$ can have at most $n - (2l+1)$ zero entries or at least $(2l+1)$ nonzero elements. Finally Theorem 4.1 gives that: with high probability, the $\mathbf{z}_0$ can be recovered by solving

$$\min_{\mathbf{z} \in \mathbb{R}^n} \|\mathcal{M}G(\mathbf{z}) - \mathbf{y}\|_0.$$

$\square$

5 Numerical Results

In this section, we present experimental results to validate our theoretical analysis. We first introduce the datasets and generative model used in our experiments. Then, we present simulation results verifying our proposed outlier detection algorithms.

We use two datasets MNIST [35] and CelebFaces Attribute (CelebA) [36] in our experiments. For generative models, we use variational auto-encoder (VAE) [28, 29] and deep convolutional generative adversarial networks (DCGAN) [20, 29].

5.1 MNIST and VAE

The MNIST database contains approximately 70,000 images of handwritten digits which are divided into two separate sets: training and test sets. The training set has 60,000 examples and the test set has 10,000 examples. Each image is of size 28×28 where each pixel is either value of '1' or '0'.

For the VAE, we adopt the pre-trained VAE generative model in [24] for MNIST dataset. The VAE system consists of an encoding and a decoding networks in the inverse architectures. Specifically, the encoding network has fully connected structure with

input, output and two hidden layers. The input has the vector size of 784 elements, the output produces the latent vector having the size of 20 elements. Each hidden layer possesses 500 neurons. The fully connected network creates 784 – 500 – 500 – 20 system. Inversely, the decoding network consists three fully connected layer converting from latent representation space to image space, i.e., 20–500–500–784 network. In the training process, the decoding network is trained in such a way to produce the similar distribution of original signals. Training dataset of 60,000 MNIST image samples was used to train the VAE networks. The training process was conducted by Adam optimizer [28] with batch size 100 and learning rate of 0.001.

When the VAE is well-trained, we exploit the decoding neural network as a generator to produce input-like signal $x' = G(\mathbf{z}) \in \mathbb{R}^n$. This processing maps a low dimensional signal $\mathbf{z} \in \mathbb{R}^k$ to a high dimensional signal $G(\mathbf{z}) \in \mathbb{R}^n$ such that $\|G(\mathbf{z}) - \mathbf{x}\|_2$ can be small, where the k is set to be 20 and $n = 784$.

Now, we solve the compressed sensing problem to find the optimal latent vector $\hat{\mathbf{z}}$ and its corresponding representation vector $G(\mathbf{z})$ by ℓ_1-norm and ℓ_2-norm minimizations which are explained as follows. For ℓ_1 minimization, we consider both the case where we solve

$$\min_{\mathbf{z} \in \mathbb{R}^k} \|\mathcal{M}G(\mathbf{z}) - \mathbf{y}\|_1 \tag{5.1}$$

by the ADMM algorithm introduced in Section 3, and the case where we solve

$$\min_{\mathbf{z} \in \mathbb{R}^k} \|\mathcal{M}G(\mathbf{z}) - \mathbf{y}\|_1^2 \tag{5.2}$$

by gradient descent (GD) algorithm [30].   We note that the optimization problem in (5.1) is non-differentiable w.r.t $\mathbf{z}$, thus, it cannot be solved by GD algorithm. The optimization problem in (5.2), however, can be solved in practice using GD algorithm. It is because (5.2) is only non-differentiable at a finite number of points. Therefore, (5.2) can be effectively solved by a numerical GD solver. In what follows, we will simply refer to the former case (5.1) as ℓ_1 ADMM and the later case (5.2) as $(\ell_1)^2$ GD. For ℓ_2 minimization, we solve the following optimization problems:,

$$\min_{\mathbf{z} \in \mathbb{R}^k} \|\mathcal{M}G(\mathbf{z}) - \mathbf{y}\|_2^2, \tag{5.3}$$

and

$$\min_{\mathbf{z} \in \mathbb{R}^k} \|\mathcal{M}G(\mathbf{z}) - \mathbf{y}\|_2^2 + \lambda\|\mathbf{z}\|_2^2. \tag{5.4}$$

Both (5.3) and (5.4) are solved by [30]. We will refer to the former case (5.3) as $(\ell_2)^2$ GD, and the later (5.4) as $(\ell_2)^2$ GD + reg. The regularization parameter λ in (5.4) is set to be 0.1.

5.2   CelebA and DCGAN

The CelebFaces Attribute dataset consists of over 200,000 celebrity images. We first resize the image samples to 64×64 RGB images, and each image will have in total 12288

pixels with values from $[-1, 1]$. We adopt the pre-trained deep convolutional generative adversarial networks (DCGAN) in [24] to conduct the experiments on CelebA dataset. Specifically, DCGAN consists of a generator and a discriminator. Both generator and discriminator have the structure of one input layer, one output layer and 4 convolutional hidden layers. We map the vectors from latent space of size $k = 100$ elements to signal space vectors having the size of $n = 64 \times 64 \times 3 = 12288$ elements.

In the training process, both the generator and the discriminator were trained. While training the discriminator to identify the fake images generated from the generator and ground truth images, the generator is also trained to increase the quality of its fake images so that the discriminator cannot identify the generated samples and ground truth image. This idea is based on Nash equilibrium [37] of game theory.

The DCGAN was trained with 200,000 images from CelebA dataset. We further use additional 64 images for testing our CS. The training process was conducted by the Adam optimizer [38] with learning rate 0.0002, momentum $\beta_1 = 0.5$ and batch size of 64 images.

Similarly, we solve our CS problems in (5.1), (5.2), (5.3) and (5.4) by ℓ_1 ADMM, $(\ell_1)^2$ GD, $(\ell_2)^2$ GD and $(\ell_2)^2$ GD + reg algorithms, respectively. The regularization parameter λ in (5.4) is set to be 0.001. Besides, we also solve the outlier detection problem by Lasso on the images in both the discrete cosine transformation domain (DCT) [39] and the wavelet transform domain (Wavelet) [40].

5.3 Experiments and Results

5.3.1 Reconstruction with various numbers of measurements

The theoretical result in [24] showed that a random Gaussian measurement $\mathcal{M}$ is effective for signal reconstruction in CS. Therefore, for evaluation, we set $\mathcal{M}$ as a random matrix with i.i.d. Gaussian entries with zero mean and standard deviation of 1. Also, every element of noise vector η is an i.i.d. Gaussian random variable. In our experiments, we carry out the performance comparisons between our proposed ℓ_1 minimization (5.1) with ADMM algorithm (referred as ℓ_1 ADMM) approaches, $(\ell_1)^2$ minimization (5.2) with GD algorithm (referred as $(\ell_1)^2$ GD), regularized $(\ell_2)^2$ minimization (5.4) with GD algorithm (referred as $(\ell_2)^2$ GD + reg), $(\ell_2)^2$ minimization (5.3) with GD algorithm (referred as $(\ell_2)^2$ GD), Lasso in DCT domain, and Lasso in wavelet domain [24]. We use the reconstruction error as our performance metric, which is defined as: error $= \|\hat{\mathbf{x}} - \mathbf{x}^*\|_2^2$, where $\hat{\mathbf{x}}$ is an estimate of $\mathbf{x}^*$ returned by the algorithm.

For MNIST, we set the standard deviation of the noise vector so that $\sqrt{\mathbb{E}[\|\eta\|^2]} = 0.1$. We conduct 10 random restarts with 1000 steps per restart and pick the reconstruction with best measurement error. For CelebA, we set the standard deviation of entries in the noise vector so that $\sqrt{\mathbb{E}[\|\eta\|^2]} = 0.01$. We conduct 2 random restarts with 500 update steps per restart and pick the reconstruction with best measurement error.

Fig.3a and Fig.3b show the performance of CS system in the presence of 3 outliers. We compare the reconstruction error versus the number of measurements for the ℓ_1-minimization based methods with ADMM (5.1) and GD (5.2) algorithms in Fig.3a. In Fig.3b, we plot the reconstruction error versus number of measurements for ℓ_2-minimization based methods with and without regularization in (5.3) and (5.4), respectively. The outliers' values and positions are randomly generated. To generate the outlier vector, we first create a vector $\mathbf{e} \in \mathbb{R}^m$ having all zero elements. Then, we randomly generate l integers in the range $[1, m]$ indicating the positions of outlier in vector $\mathbf{e}$. Now, for each generated outlier position, we assign a large random value in the range [5000, 10000]. The outlier vector $\mathbf{e}$ is then added into CS model as in (1.1). As we can see in Fig.3a when ℓ_1 minimization algorithms (ℓ_1 ADMM and $(\ell_1)^2$ GD) were used, the reconstruction errors fast converge to low values as the number of measurements increases. On the other hand, the ℓ_2-minimization based recovery do not work well as can be seen in Fig.3b even when number of measurements increases to a large quantity. One observation can be made from Fig.3a is that after 100 measurements, our algorithm's performance saturates, higher number of measurements does not enhance the reconstruction error performance. This is because of the limitation of VAE architecture.

Similarly, we conduct our experiments with CelebA dataset using the DCGAN generative model. In Fig. 4a, we show the reconstruction error change as we increase the number of measurements both for ℓ_1-minimization based with the ℓ_1 ADMM and $(\ell_1)^2$ GD algorithms. In Fig. 4b, we compare reconstruction errors of ℓ_2-minimization using GD algorithms and Lasso with the DCT and wavelet bases. We observed that in the presence of outliers, ℓ_1-minimization based methods outperform the ℓ_2-minimization based algorithms and methods using Lasso.

We plot the sample reconstructions by Lasso and our algorithms in Fig. 5. We observed that ℓ_1 ADMM and $(\ell_1)^2$ GD approaches are able to reconstruct the images with only as few as 100 measurements while conventional Lasso and ℓ_2 minimization algorithm are unable to do the same when number of outliers is as small as 3.

For CelebA dataset, we first show the reconstruction performance when the number of outlier is 3 and the number of measurements is 500. We plot the reconstruction results using ℓ_1 ADMM and $(\ell_1)^2$ GD algorithms with DCGAN in Fig. 6. Lasso DCT and Wavelet, $(\ell_2)^2$ GD and $(\ell_2)^2$ GD + reg with DCGAN reconstruction results are showed in Fig. 7. Similar to the result in MNIST set, the proposed ℓ_1-minimization based algorithms with DCGAN perform better in the presence of outliers. This is because ℓ_1-minimization-based approaches can successfully eliminate the outliers while ℓ_2-minimization-based methods do not.

We show further results for both two datasets with various numbers of measurements in Fig. 8, 9, 10, and 11. Specifically, Fig. 8 shows MNIST reconstruction results using ℓ_1-minimization based algorithms, and Fig. 9 plots MNIST reconstruction results using ℓ_2-minimization based algorithm and Lasso, respectively. Fig. 10, and 11 display sample results for CelebA recovery with different algorithms.

5.3.2 Reconstruction with different numbers of outliers

Now, we evaluate the recovery performance of CS system under different numbers of outliers. We first fix the noise levels for MNIST and CelebA as the same as in the previous experiments. Then, for each dataset, we vary the number of outliers from 5 to 50, and measure the reconstruction error per pixel with various numbers of measurements. In these evaluations, we use ℓ_1-minimization based algorithms (ℓ_1 ADMM and $(\ell_1)^2$ GD) for outlier detection and image reconstruction.

For MNIST dataset, we plot the reconstruction error performance for 5, 10, 25 and 50 outliers, respectively, in Fig. 12. One can be seen from Fig. 12 that as the number of outliers increases, larger number of measurements are needed to guarantee successful image recovery. Specifically, we need at least 25 measurements to lower error rate to below 0.08 per pixel when there are 5 outliers in data, while the number of measurements should be tripled to obtain the same performance in the presence of 50 outliers. We show the image reconstruction results using ADMM and GD algorithms with different numbers of outliers in Fig. 14.

Next, for the CelebA dataset, we plot the reconstruction error performance for 5, 10, 25 and 50 outliers in Fig. 13. We compare the image reconstruction results using ℓ_1 ADMM and $(\ell_1)^2$ GD algorithms in Fig. 15.

6   Conclusions and Future Directions

In this paper, we investigated solving the outlier detection problems via a generative model approach. This new approach outperforms the ℓ_2 minimization and traditional Lasso in both the DCT domain and Wavelet domain. The iterative alternating direction method of multipliers we proposed can efficiently solve the proposed nonlinear ℓ_1 norm-based outlier detection formulation for generative model. Our theory shows that for both the linear neural networks and nonlinear neural networks with arbitrary number of layers, as long as they satisfy certain mild conditions, then with high probability, one can correctly detect the outlier signals based on generative models.

References

[1] E. Candes, J. Romberg, and T. Tao. Robust uncertainty principles: exact signal reconstruction from highly incomplete frequency information. *IEEE Trans. on Inform. Theory*, 52(2):489–509, Feb 2006.

[2] D. Donoho. Compressed sensing. *IEEE Trans. Inf. Theor.*, 52(4):1289–1306, April 2006.

[3] E. Candes and B. Recht. Exact matrix completion via convex optimization. *Foundations of Computational Mathematics*, 9(6):717, Apr 2009.

[4] M. Lustig, D. Donoho, and J. Pauly. Sparse mri: the application of compressed sensing for rapid mr imaging. *Magnetic Resonance in Medicine*, 58(6):1182–1195, 2007.

[5] O. Jaspan, R. Fleysher, and M. Lipton. Compressed sensing mri: a review of the clinical literature. *The British Journal of Radiology*, 88(1056):20150487, 2015. PMID: 26402216.

[6] W. Xu, J. Yi, S. Dasgupta, J. Cai, M. Jacob, and M. Cho. Separation-free super-resolution from compressed measurements is possible: an arthonormal atomic norm minimization approach. *arXiv:1711.01396 [cs, math]*, November 2017. arXiv: 1711.01396.

[7] J. Cai, X. Qu, W. Xu, and G. Ye. Robust recovery of complex exponential signals from random Gaussian projections via low rank Hankel matrix reconstruction. *Applied and Computational Harmonic Analysis*, 41(2):470–490, September 2016.

[8] J. Bobin, J. Starck, and R. Ottensamer. Compressed sensing in astronomy. *IEEE Journal of Selected Topics in Signal Processing*, 2(5):718–726, October 2008.

[9] K. Mitra, A. Veeraraghavan, and R. Chellappa. Analysis of sparse regularization based robust regression approaches. *IEEE Transactions on Signal Processing*, 61(5):1249–1257, March 2013.

[10] R. E. Carrillo, K. E. Barner, and T. C. Aysal. Robust sampling and reconstruction methods for sparse signals in the presence of impulsive noise. *IEEE Journal of Selected Topics in Signal Processing*, 4(2):392–408, April 2010.

[11] C. Studer, P. Kuppinger, G. Pope, and H. Bolcskei. Recovery of sparsely corrupted signals. *IEEE Transactions on Information Theory*, 58(5):3115–3130, May 2012.

[12] W. Xu, M. Wang, J. F. Cai, and A. Tang. Sparse error correction from nonlinear measurements with applications in bad data detection for power networks. *IEEE Transactions on Signal Processing*, 61(24):6175–6187, December 2013.

[13] E. Bai. Outliers in system identification. In *2017 IEEE 56th Annual Conference on Decision and Control (CDC)*, pages 4130–4134, December 2017.

[14] K. Barner and G. Arce. *Nonlinear signal and image processing: theory, methods, and applications*. CRC Press, 2003.

[15] E. J. Candes and T. Tao. Decoding by linear programming. *IEEE Trans. on Information Theory*, 51(12):4203–4215, Dec 2005.

[16] J. Wright and Y. Ma. Dense error correction via ℓ_1-minimization. *IEEE Transactions on Information Theory*, 56(7):3540–3560, July 2010.

[17] Q. Wan, H. Duan, J. Fang, H. Li, and Z. Xing. Robust Bayesian compressed sensing with outliers. *Signal Processing*, 140:104–109, November 2017.

[18] B. Popilka, S. Setzer, and G. Steidl. Signal recovery from incomplete measurements in the presence of outliers. *Inverse Problems and Imaging*, 1(4):661, 2007.

[19] E. J. Candes and P. A. Randall. Highly robust error correction by convex programming. *IEEE Transactions on Information Theory*, 54(7):2829–2840, July 2008.

[20] I. Goodfellow, Y. Bengio, and A. Courville. *Deep learning*. MIT Press, 2016. http://www.deeplearningbook.org.

[21] Y. Yang, J. Sun, H. Li, and Z. Xu. ADMM-net: a deep learning approach for compressive sensing MRI. *arXiv:1705.06869 [cs]*, May 2017. arXiv: 1705.06869.

[22] C. Metzler, A. Mousavi, and R. Baraniuk. Learned D-AMP: a principled CNN-based compressive image recovery algorithm. *arXiv:1704.06625 [cs, stat]*, April 2017. arXiv: 1704.06625.

[23] H. Gupta, K. H. Jin, H. Q. Nguyen, M. T. McCann, and M. Unser. CNN-based projected gradient descent for consistent CT image reconstruction. *IEEE Transactions on Medical Imaging*, 37(6):1440–1453, June 2018.

[24] A. Bora, A. Jalal, E. Price, and A. Dimakis. Compressed sensing using generative models. *arXiv:1703.03208 [cs, math, stat]*, March 2017. arXiv: 1703.03208.

[25] M. Dhar, A. Grover, and S. Ermon. Modeling sparse deviations for compressed sensing using generative models. *arXiv:1807.01442 [cs, stat]*, July 2018. arXiv: 1807.01442.

[26] S. Wu, A. Dimakis, S. Sanghavi, F. Yu, D. Holtmann-Rice, Dmitry Storcheus, Afshin Rostamizadeh, and Sanjiv Kumar. The sparse recovery autoencoder. *arXiv:1806.10175 [cs, math, stat]*, June 2018. arXiv: 1806.10175.

[27] V. Papyan, Y. Romano, J. Sulam, and M. Elad. Theoretical foundations of deep learning via sparse representations: a multilayer sparse model and its connection to convolutional neural networks. *IEEE Signal Processing Magazine*, 35(4):72–89, July 2018.

[28] D. Kingma and M. Welling. Auto-encoding variational Bayes. *ArXiv e-prints*, December 2013.

[29] I. Goodfellow, J. Pouget-Abadie, M. Mirza, B. Xu, D. Warde-Farley, S. Ozair, A. Courville, and Y. Bengio. Generative adversarial nets. In Z. Ghahramani, M. Welling, C. Cortes, N. D. Lawrence, and K. Q. Weinberger, editors, *Advances in Neural Information Processing Systems 27*, pages 2672–2680. Curran Associates, Inc., 2014.

[30] Jonathan Barzilai and Jonathan M. Borwein. Two-point step size gradient methods. *IMA Journal of Numerical Analysis*, 8(1):141–148, 1988.

[31] M. Abadi, P. Barham, J. Chen, Z. Chen, A. Davis, J. Dean, M. Devin, S. Ghemawat, G. Irving, and M. Isard. Tensorflow: a system for large-scale machine learning. In *OSDI*, volume 16, pages 265–283, 2016.

[32] S. Boyd, N. Parikh, E. Chu, B. Peleato, and J. Eckstein. Distributed optimization and statistical learning via the alternating direction method of multipliers. *Found. Trends Mach. Learn.*, 3(1):1–122, January 2011.

[33] R. Zippel. *Effective polynomial computation*, volume 241. Springer Science & Business Media, 2012.

[34] M. Khajehnejad, A. Dimakis, W. Xu, and B. Hassibi. Sparse recovery of nonnegative signals with minimal expansion. *IEEE Trans. on Signal Processing*, 59(1), 2011.

[35] Y. Lecun, L. Bottou, Y. Bengio, and P. Haffner. Gradient-based learning applied to document recognition. *Proceedings of the IEEE*, 86(11):2278–2324, Nov 1998.

[36] Z. Liu, P. Luo, X. Wang, and X. Tang. Deep learning face attributes in the wild. In *2015 IEEE International Conference on Computer Vision (ICCV)*, pages 3730–3738, Dec 2015.

[37] John F. Nash. Equilibrium points in n-person games. *Proceedings of the National Academy of Sciences*, 36(1):48–49, 1950.

[38] D. Kingma and J. Ba. Adam: a method for stochastic optimization. *CoRR*, abs/1412.6980, 2014.

[39] N. Ahmed, T. Natarajan, and K. R. Rao. Discrete cosine transfom. *IEEE Trans. Comput.*, 23(1):90–93, January 1974.

[40] Ingrid Daubechies. Orthonormal bases of compactly supported wavelets. *Communications on Pure and Applied Mathematics*, 41(7):909–996, 1988.

(a) ℓ_1- minimization algorithms

(b) ℓ_2- minimization algorithms
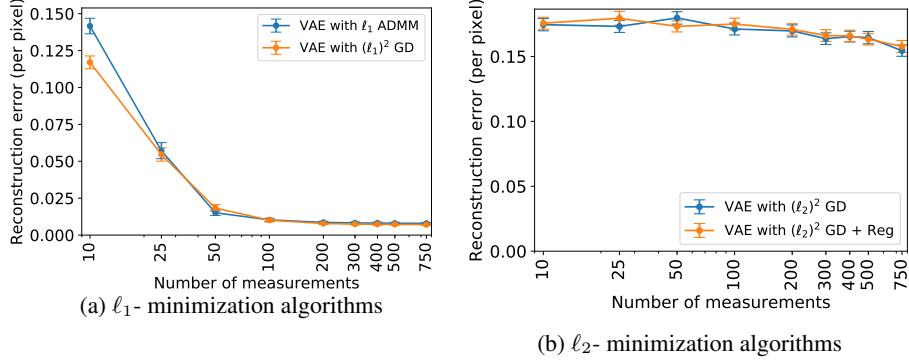
Figure 3: MNIST results: We compare the reconstruction error performance using VAE among ℓ_1 ADMM algorithm solving (5.1), $(\ell_1)^2$ GD algorithm solving (5.2), $(\ell_2)^2$ GD algorithm solving (5.3) and $(\ell_2)^2$ GD + reg algorithm solving (5.4). We plot the reconstructions error per pixel versus various numbers of measurements when the number of outliers is 3. The vertical bars indicate 95% confidence intervals.

(a) ℓ_1- minimization algorithms

(b) ℓ_2- minimization algorithm and lasso methods
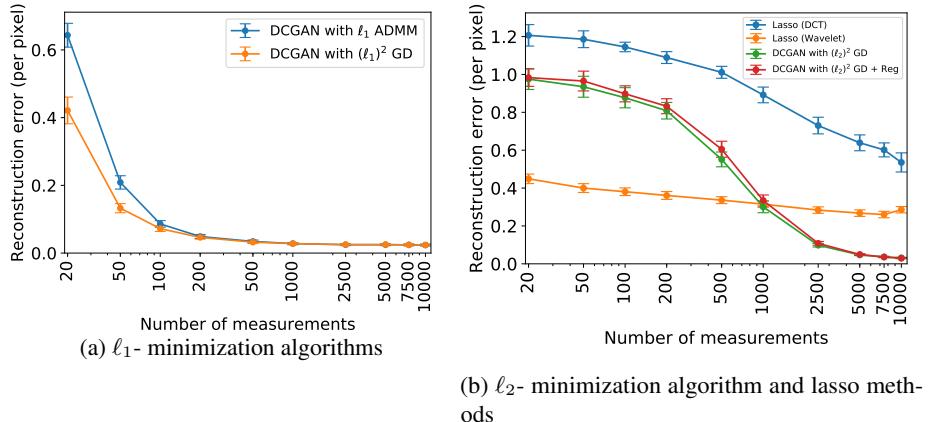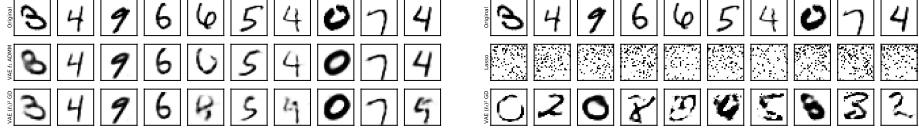
Figure 4: CelebA results: We compare the reconstruction error performance using DCGAN among ℓ_1 ADMM algorithm solving (5.1), $(\ell_1)^2$ GD algorithm solving (5.2), $(\ell_2)^2$ GD algorithm solving (5.3), $(\ell_2)^2$ GD + regularization algorithm solving (5.4), and Lasso with DCT and Wavelet bases methods. We plot the reconstructions error per pixel versus various numbers of measurements when the number of outliers is 3. The vertical bars indicate 95% confidence intervals.

29

(a) Top row: original images, middle row: re-constructions by VAE with ℓ_1 ADMM algorithm, and bottom row: reconstructions by VAE with $(\ell_1)^2$ GD algorithm.

(b) Top row: original images, middle row: re-constructions by Lasso, and bottom row: reconstructions by VAE with $(\ell_2)^2$ GD algorithm.
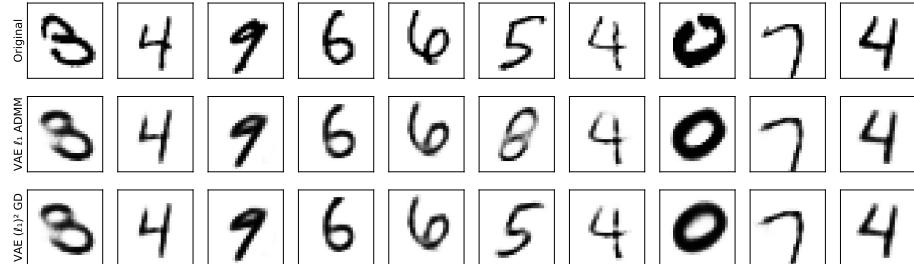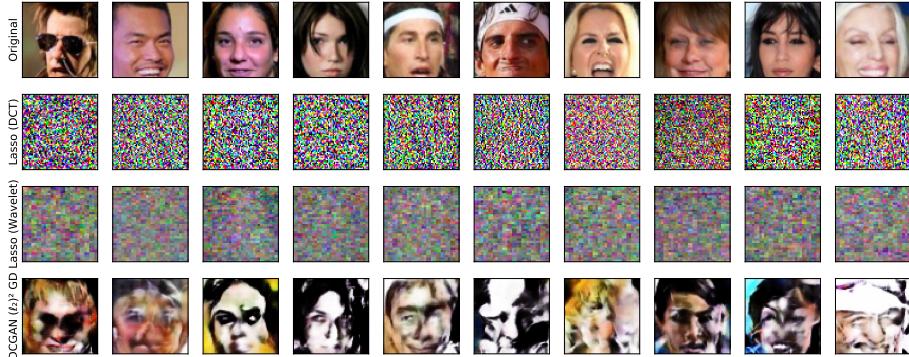
Figure 5: Reconstructions of MNIST samples when the number of measurements is 100 and the number of outliers is 3
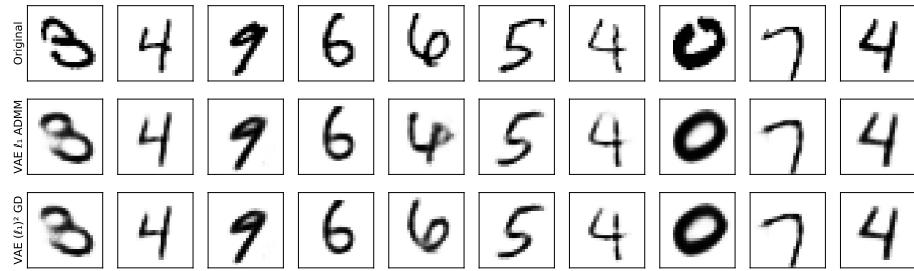
Figure 6: Reconstruction results of CelebA samples when the number of measurements is 500 and the number of outliers is 3. Top row: original images, middle row: reconstructions by DCGAN with ℓ_1 ADMM algorithm, and bottom row: reconstructions by DCGAN with $(\ell_1)^2$ GD algorithm.
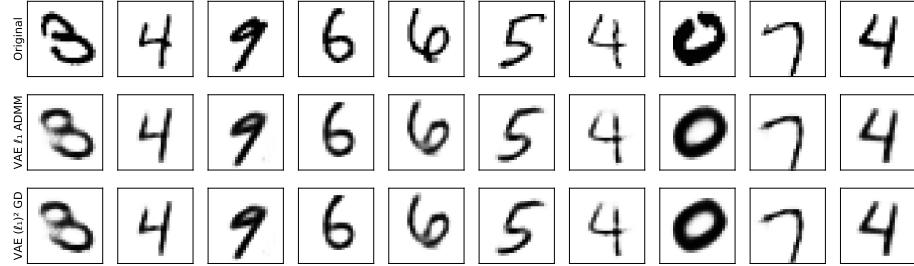
Figure 7: Reconstruction results of CelebA samples when the number of measurements is 500 and the number of outliers is 3. Top row: original images, middle row: reconstructions by Lasso with DCT basis, Third row: reconstructions by Lasso with wavelet basis, and last row: reconstructions by DCGAN with $(\ell_2)^2$ GD algorithm.
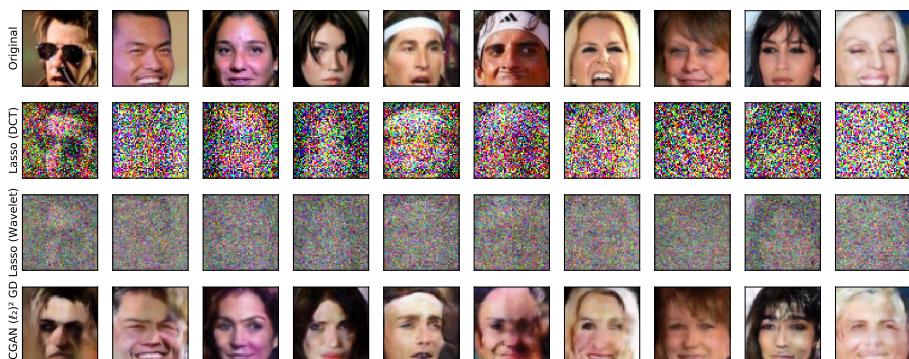
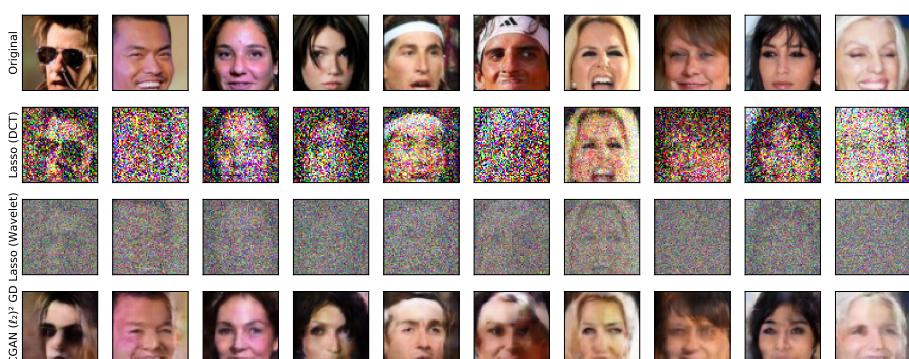(a) 200 measurements
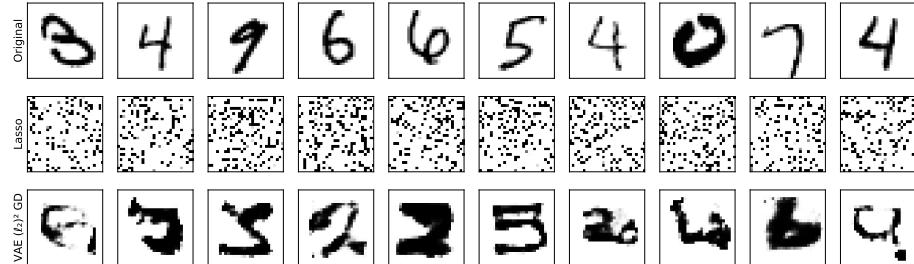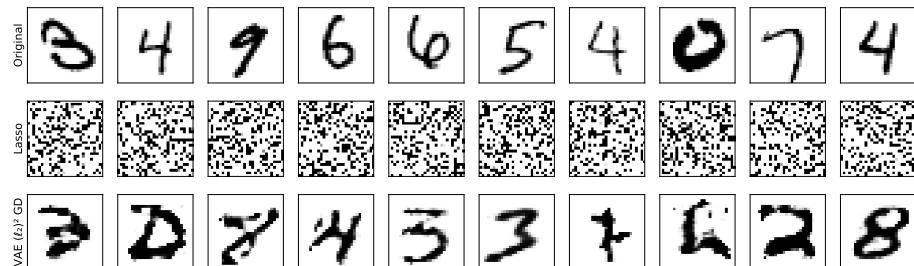
(b) 400 measurements
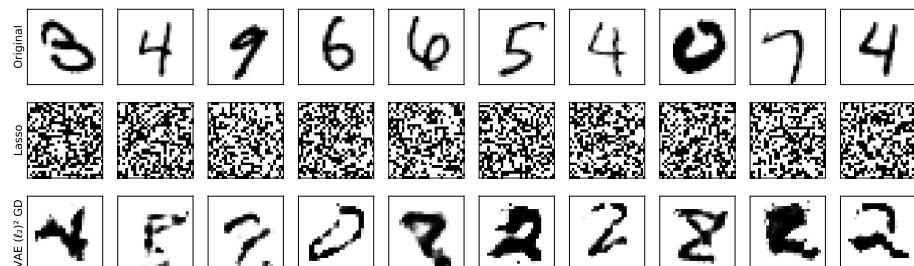
(c) 750 measurements

Figure 8: Reconstruction results of MNIST samples with different numbers of measurements when the number of outliers is 3. Note that in each result, top row: original images, middle row: reconstructions by VAE with ℓ_1 ADMM algorithm, and bottom row: reconstructions by VAE with $(\ell_1)^2$ GD algorithm.

(a) 200 measurements

(b) 400 measurements

(c) 750 measurements

Figure 9: Reconstruction results of MNIST samples with different numbers of measurements when the number of outliers is 3 (continue). Note that in each result, top row: original images, middle row: reconstructions by Lasso, and bottom row: reconstructions by VAE with $(\ell_2)^2$ GD algorithm.

32

(a) 1000 measurements

(b) 5000 measurements

(c) 10000 measurements

Figure 10: Reconstruction results of CelebA samples with different numbers of measurements when the number of outliers is 3. Note that in each result, top row: original images, middle row: reconstructions by DCGAN with ℓ_1 ADMM algorithm, and bottom row: reconstructions by DCGAN with $(\ell_1)^2$ GD algorithm.

(a) 1000 measurements

(b) 5000 measurements

(c) 10000 measurements

Figure 11: Reconstruction results of CelebA samples with different numbers of measurements when the number of outliers is 3 (continue). In each row of results, top row: original images, second row: reconstructions by Lasso with DCT basis, third row: reconstructions by Lasso with wavelet basis, and last row: reconstructions by DCGAN with $(\ell_2)^2$ GD algorithm.
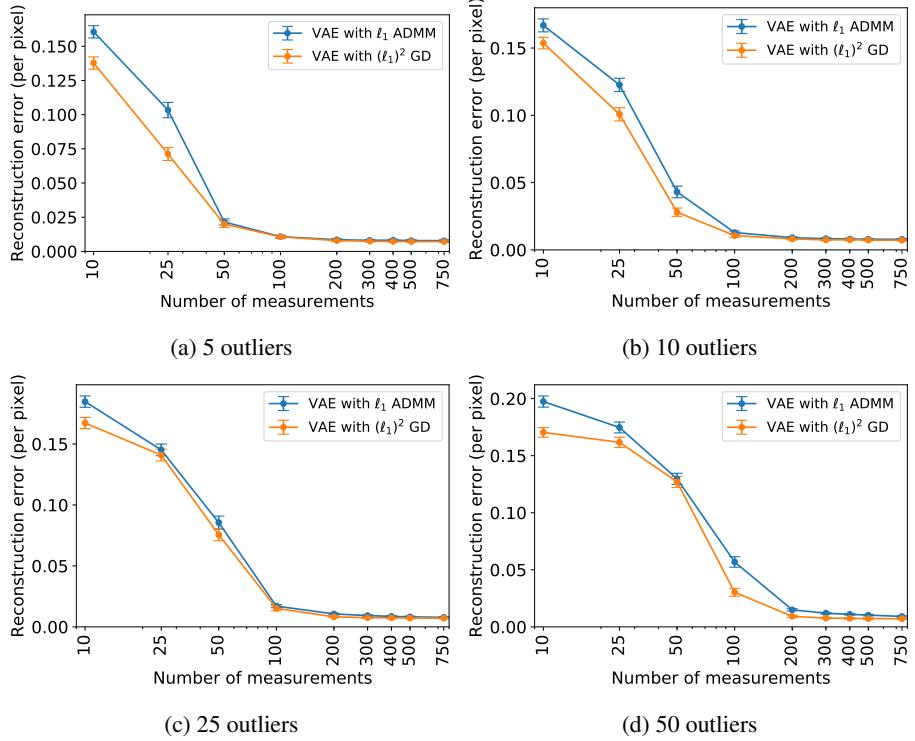
(a) 5 outliers

(b) 10 outliers

(c) 25 outliers

(d) 50 outliers

Figure 12: MNIST results: We compare the reconstruction error performance for VAE with ℓ_1 ADMM and $(\ell_1)^2$ GD algorithms with different numbers of outliers.

(a) 5 outliers
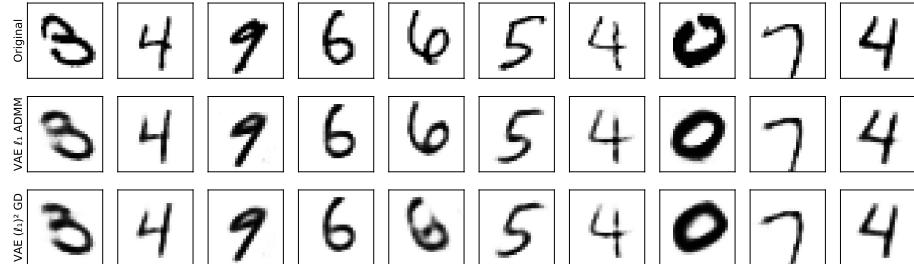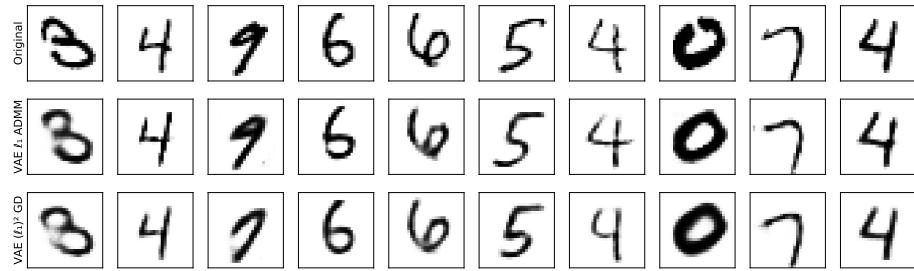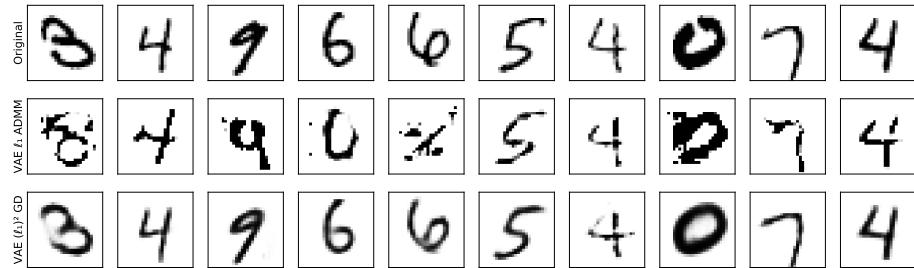
(b) 10 outliers

(c) 25 outliers
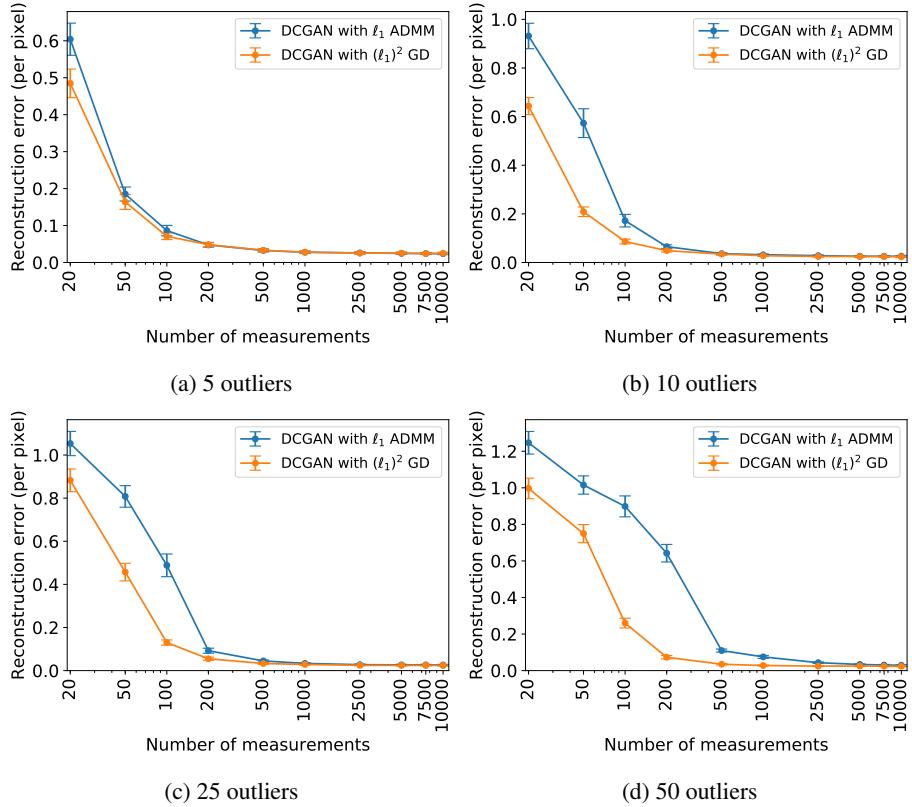
(d) 50 outliers

Figure 13: CelebA results: We compare the the reconstruction error performance for DCGAN with ℓ_1 ADMM and $(\ell_1)^2$ GD algorithms with different numbers of outliers.

(a) 5 outliers

(b) 10 outliers

(c) 25 outliers

Figure 14: Reconstruction results of MNIST samples with different numbers of outliers when the number of measurements is 100. In each set of results, top row: original images, middle row: reconstructions by VAE with ℓ_1 ADMM algorithm, and bottom row: reconstructions by VAE with $(\ell_1)^2$ GD algorithm.

(a) 5 outliers
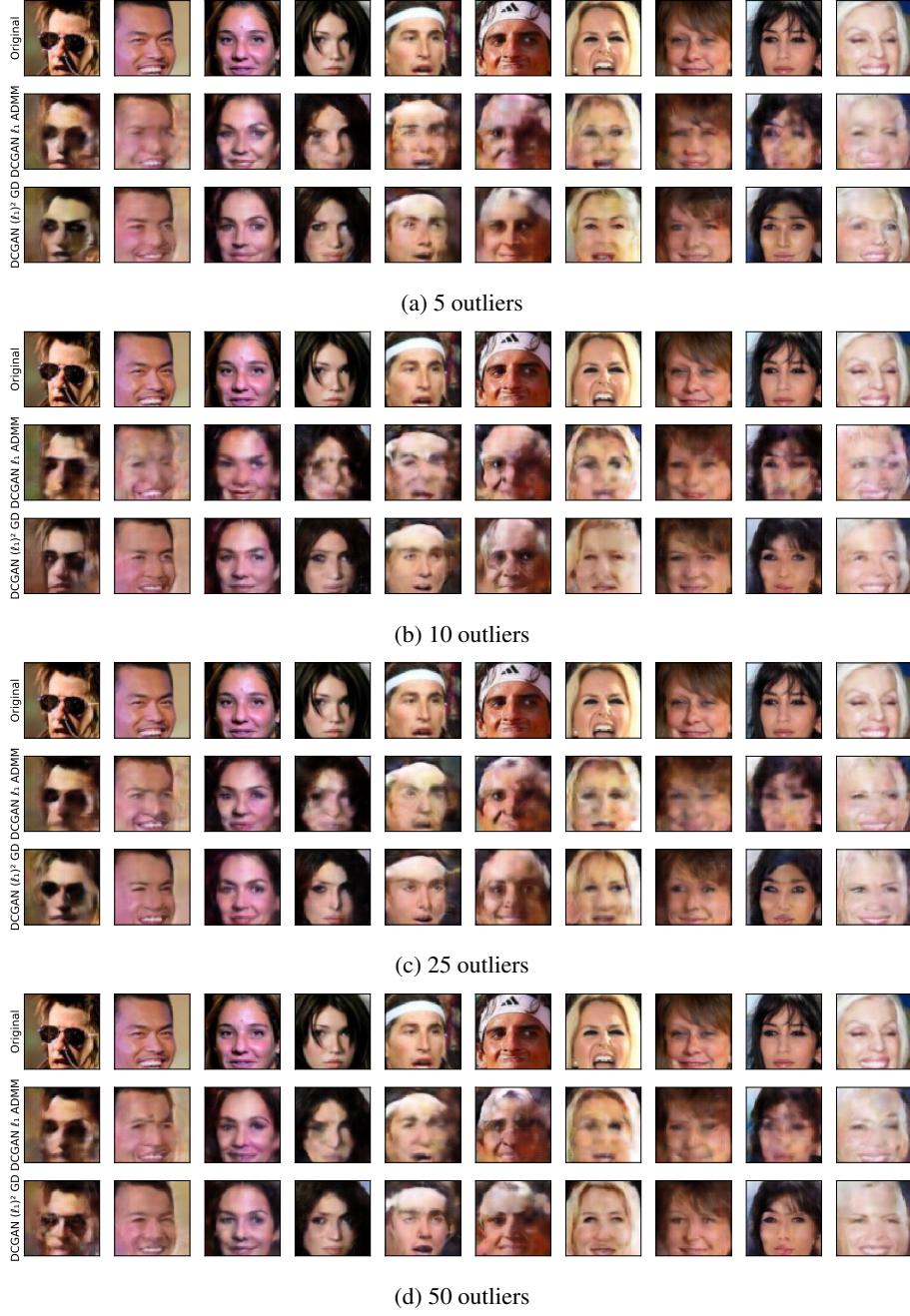

(b) 10 outliers

(c) 25 outliers

(d) 50 outliers

Figure 15: Reconstruction results of CelebA samples with different numbers of outliers when the number of measurements is 1000. In each set of results, top row: original images, middle row: reconstructions by DCGAN with ℓ_1 ADMM algorithm, and bottom row: reconstructions by DCGAN with $(\ell_1)^2$ GD algorithm.